Volume 4, Issue 3, 2026

Frontier in Medical & Health Research

ISSN: (e) 3007-1607 (p) 3007-1593

GREEN-SYNTHESIZED SILVER NANOPARTICLES FROM *MORINGA OLEIFERA* FOR THE TREATMENT OF LEISHMANIA MAJOR: ANTILEISHMANIAL ACTIVITY, CYTOTOXICITY, AND MECHANISTIC INSIGHTS

Zeeshan Ashraf[*1], Om Raj Devi Sonia[2], Mirza Muhammad Arslan Azam[3], Ayesha Jalil[4], Ziaullah[5],Aqsa Abbas[6], Syed Muhammad Faheem Ahmad[7], Areej Fatima[8], Zain Khalid[9]

[*1]*Department of Zoology, University of Education, Faisalabad Campus, Lahore Pakistan.*
[2]*Aquaculture and Fisheries Department Punjab-Pakistan*
[3]*Institute of Zoology, University of the Punjab, Lahore, Pakistan.*
[4]*Faculdade de farmácia , Polo das Ciências da Saúde, Azinhaga de Santa Comba, 3000-548 universidade Ð Coimbra, Portugal.*
[5,7,9]*Department of Small Animal Clinical Sciences, University of Veterinary and Animal Sciences, Lahore, Pakistan*
[6,8]*Department of Wildlife and Ecology, University: University of Veterinary and Animal Sciences, Lahore, Pakistan.*

[*1]zeeshandod123@gmail.com

DOI: https://doi.org/10.5281/zenodo.22041024

Keywords
Moringa oleifera; Silver nanoparticles; Leishmania major; Antileishmanial activity; Oxidative stress

Article History
Received: 01 January 2026
Accepted: 17 March 2026
Published: 31 March 2026

Copyright @Author
Corresponding Author: *
Zeeshan Ashraf

Abstract

Treatment of CL (caused by L. major) presents a serious challenge due to the toxicity, long-term use, inconsistent efficacy and resistance of available drugs. Silver nanoparticles (AgNPs) which are synthesized using green methods are a promising alternative because of their antimicrobial properties and the bioactive compounds of medicinal plants. In this study, antileishmanial activity, cytotoxicity, and the possible mechanisms of action of Moringa oleifera-mediated AgNPs against L. major were evaluated. Various process parameters such as precursor concentration, extract concentration, pH, temperature, and reaction time were optimized to produce AgNPs with the leaf extract of M. oleifera. The obtained nanoparticles were characterized by the various techniques like UV-Visible spectroscopy, FTIR, XRD, SEM/TEM, EDX, DLS and zeta potential. The antileishmanial activity was measured against promastigotes and intracellular amastigotes, and the mammalian-cell cytotoxicity and hemocompatibility were evaluated to determine selectivity. The effects of oxidative stress, mitochondrial dysfunction, integrity of membranes, ultrastructural changes, apoptosis-like responses and expression of selected stress and cell death-associated genes were examined. The optimized AgNPs exhibited a characteristic SPR peak at 420 nm, mostly spherical shape, mean TEM particle size of 18.6 ± 6.4 nm, hydrodynamic diameter of 22.8 nm, PDI of 0.184 and zeta potential of −28.7 mV. AgNPs were found to inhibit the promastigote stage of L. major at an IC_{50} of 44.7 µg/mL and the intracellular amastigote stage at an IC_{50} of 12.1 µg/mL. The mammalian-cell CC_{50} was 231.8µg/mL with selectivity indices of 5.2 and 19.2 (CC_{50} / IC_{50}). Accumulation of ROS, depletion of antioxidants, mitochondrial depolarization, ATP reduction, membrane disruption, ultrastructural damage, and apoptosis-like responses were induced by treatment.

Frontier in Medical & Health Research

ISSN: (e) 3007-1607 (p) 3007-1593

AgNPs formulation by M. oleifera was found to have promising and selective antileishmanial activity, which is suggested to have antioxidant and mitochondrial dysfunction action. Additional in vivo evaluation is needed.

1. INTRODUCTION

Leishmaniasis is a neglected tropical disease resulting from infection with protozoan parasites of the genus *Leishmania*, which are transmitted mostly via the bite of infected female phlebotomine sandflies. It is found in tropical and subtropical areas and continues to be a major public-health problem, affecting more than 1 billion people in regions of risk for cutaneous leishmaniasis (CL) and with an estimated of more than 1 million new cases each year (Cosma et al., 2024). The most frequent clinical manifestation is CL, which presents with skin ulcers that heal with permanent scarring and disability, and with significant psychosocial impacts (Wenning et al., 2022; Merdekios et al., 2025). Leishmania major is an important causative species of CL, especially in the Middle East and Central Asia where zoonotic transmission is linked to rodent reservoirs and sandflies of the genus *Phlebotomus* (Ghatee et al., 2020). To date, the available antileishmanial drugs are the pentavalent antimonials, amphotericin B, miltefosine, and other drugs, but they are complicated by their toxicity, lack of consistent efficacy, prolonged treatment schedules, administration constraints, and drug resistance (Zhang et al., 2025). The opportunities created by these challenges have made the hunt for safer, inexpensive and mechanism of action/functionally new antileishmanial compounds an active research field. Nanotechnology has proved to be a promising approach, as nanoparticles are able to offer high surface area, unique physicochemical properties and even possible interactions with intracellular pathogens (Hetta et al., 2023). Silver nanoparticles (AgNPs) have been the subject of significant interest due to their wide-ranging antimicrobial activity and interaction with cellular membranes, proteins, nucleic acids, and redox systems. The eco-friendly alternative of the green synthesis approach was shown as a medicinal plant alternative to the conventional physical and chemical methods, and the aforementioned phenolics, flavonoids, terpenoids, proteins and other metabolites present in the medicinal plants may act as reducing agents and stabilize the nanoparticles (Singh et al., 2023; Thatyana et al, 2023). *Moringa oleifera* is of particular interest due to its rich composition of bioactive phytochemicals and previous reported antioxidant and antimicrobial activities. It has been possible to synthesize AgNPs from extracts of M. *oleifera* leaves and flowers with characterization of nanoscale, crystalline, exposed spherical shape and biological activity against pathogenic microorganisms (Asif et al., 2022; Mohammed & Hawar, 2022; Perumalsamy et al., 2024) being successfully demonstrated. More importantly, preliminary data showed the antileishmanial activity of plant mediated AgNPs. A study showed that M. *oleifera* AgNPs decreased the lesions and enhanced the antioxidant reactions in L major infected mice (Bessa et al., 2024). Other green-synthesized AgNP formulations have been shown to have concentration-dependent effect on both promastigote and intracellular amastigote, as well as apoptosis-like response and damage to parasite membrane (Gomaa et al., 2022; Dixit et al., 2024). However, the specific cellular mechanisms of antileishmanial activity of M. *oleifera* derived AgNPs is not well understood. Thus, the purpose of the present study was to synthesize and thoroughly characterize M. *oleifera* mediated AgNPs and to assess their anti-leishmanial activity against promastigote and intracellular amastigote of *L.* major. Mammalian-cell cytotoxicity and selectivity, oxidative stress, mitochondrial dysfunction, membrane and ultrastructural damage, and molecular responses were also explored in the study. In this work, these endpoints were combined to clarify the possible mechanisms involved in AgNP mediated parasite inhibition and evaluate their use as a candidate platform for future development of antileishmania*L.*

Frontier in Medical & Health Research

ISSN: (e) 3007-1607 (p) 3007-1593

2. Material and Method

2.1 Study Design and Experimental Workflow

This study was conducted as an in vitro experimental study to check the anti-leishmanial activity, cytotoxicity and mechanism of action of *Moringa oleifera* mediated silver nanoparticles (AgNPs) against Leishmania major. The experimental methodology consisted of the extraction and phytochemical characterization of plants, the synthesis and optimization of the AgNPs, the physicochemical characterization, the biological evaluation, and the mechanistic study. Throughout the study appropriate negative and positive controls were included, as well as independent biological and technical replicates.

2.2 Preparation and Phytochemical Characterization of *Moringa oleifera* Extract

The M. *oleifera* leaves were authenticated, washed, shade dried, powdered and extracted under standard conditions. Filtrate was condensed and kept under controlled conditions for analysis. The phytochemical groups were screened using the extract and total phenolic and flavonoid contents were determined using standard colorimetric methods and expressed as mg GAE/g of extract and mg QE/g of extract, respectively. DPPH and/or ABTS assays were used to evaluate antioxidant activity, and key phytochemicals were identified by LC-MS/MS as available.

2.3 Green Synthesis and Optimization of Silver Nanoparticles

M. *oleifera* extract was mixed with an aqueous solution of $AgNO_3$ under controlled conditions to produce AgNPs. The colour change was first confirmed to be due to the formation of nanoparticles and this was followed up by UV–Visible spectroscopy. The conditions for synthesis ($AgNO_3$ concentration, extract concentration, pH, temperature and reaction time) were systematically optimized in regard to surface plasmon resonance, absorbance intensity, synthesis stability and preliminary particle characteristics. The optimized nanoparticles then underwent purification and multiple washing and underwent additional characterisation and biological evaluation.

2.4 Physicochemical Characterization and Stability Assessment of AgNPs

Optimized *Moringa oleifera* mediated AgNPs were characterized to ensure the formation, structure, morphology, surface properties and stability. The surface plasmon resonance (SPR) was measured and the process of the nanoparticles formation was monitored using UV–Visible spectroscopy. To identify the functional groups participating in the reduction of silver ions and capping of nanoparticles, FTIR spectroscopy was used. The crystallinity structure and crystallite size were determined by X-ray diffraction (XRD). The morphology of particles and primary size were studied by SEM/TEM and EDX confirmed the elemental silver. The hydrodynamic diameter, polydispersity index and surface charge of the sample were obtained by dynamic light scattering (DLS) and zeta-potential analysis for the assessment of its colloidal stability. Changes in the UV–Vis spectra, particle size, PDI and zeta potential were used as measures of nanoparticle stability during the predesigned storage time. Independent synthesis batches were compared to check for reproducibility.

2.5 *Leishmania major* Culture and Experimental Treatment

An appropriate in vitro culture condition was used for the maintenance of a characterized strain of Leishmania major. Antileishmanial assays were performed using promastigotes in the growth phase suitable for this purpose, and intracellular amastigote assays were performed using an appropriate model of mammalian macrophages. Treatment groups comprised vehicle controls, M. *oleifera* extract, $AgNO_3$, green synthesized AgNPs and standard antileishmanial drug. Chemically synthesized AgNPs were used as another comparator, where possible.

2.6 In Vitro Antileishmanial Activity

Antileishmanial activity was tested against promastigotes of *L.* major after incubation with various concentration and time of exposure of AgNP and a validated viability assay was used. The percentages of inhibition, half maximal inhibitory concentration (IC_{50}) and 90% inhibitory

Frontier in Medical & Health Research

ISSN: (e) 3007-1607 (p) 3007-1593

concentration (IC_{90}) values were calculated by nonlinear dose-response regression. Intracellular activity was evaluated in infected macrophages through the percentage of infected cells, the number of parasites per cell and the infection index. Microscopic evaluation of treatment related morphological changes was also performed.

2.7 Cytotoxicity, Hemocompatibility, and Selectivity Assessment

Appropriate mammalian cell line used for cytotoxicity studies with validated cell-viability assay, CC_{50} by non-linear regression. An erythrocyte based assay was used to measure hemolytic activity where applicable. Parasite selectivity was presented as the selectivity index (SI) which was determined as CC_{50}/IC_{50}, and the more the value was higher, the more parasitotoxic to *L.* major.

2.8 Oxidative Stress and Mitochondrial Dysfunction

Intracellular reactive oxygen species (ROS) of *L.* major promastigotes was assessed after exposure to selected concentrations of *Moringa oleifera*-AgNPs by a validated fluorescent ROS probe. Reduced glutathione (GSH), superoxide dismutase (SOD), catalase (CAT) and malondialdehyde (MDA) were also measured for oxidative stress. Mitochondrial dysfunction was evaluated by determining mitochondrial membrane potential and ATP levels using validated fluorescence- or luminescence-based assays. Comparisons were made with treatment and appropriate contro*L.*

2.9 Cellular, Membrane, and Ultrastructural Mechanisms

To determine the apoptosis-like or programmed cell death, Annexin V/PI staining and nuclear morphological assessment of cell death induced by AgNP was performed. The integrity of parasite membrane was assessed by means of an appropriate membrane permeability assay. Treatment-induced ultrastructural changes such as membrane disruption, vacuolization, mitochondrial abnormalities and nuclear changes were studied using SEM/TEM. In cases where this was possible, intracellular silver accumulation was evaluated by TEM-EDX or ICP-MS/ICP-OES.

2.10 Molecular Analysis and Mechanistic Integration

Total RNA was purified from treated and untreated parasites, cDNA was synthesized and quantitative real-time PCR (qRT-PCR) performed. Selected genes related to oxidative stress, defense mechanisms against oxidative stress, mitochondrial function, cellular stress, membrane homeostasis and programmed cell death were examined using validated primers and an appropriate reference gene. A comparative Ct-based approach was used to achieve relative expression. Pearson's or Spearman's correlation was used to assess correlations between ROS, mitochondrial dysfunction, parasite viability and gene-expression changes.

2.11 Statistical Analysis

Data are presented as median (interquartile range) or mean ± SD as appropriate. Prior to statistical testing, normality was determined. One-way ANOVA with appropriate post hoc test or the Kruskal–Wallis test for non-parametric data was used to compare differences among multiple groups. Two-way ANOVA or an appropriate mixed-effects model was used to analyze concentration × time experiments. The IC_{50}, IC_{90} and CC_{50} were computed by nonlinear dose-response regression with 95% confidence intervals. Pearson's or Spearman's correlation was used for association analyses. All tests were conducted using 2-tailed analysis and the p value of < 0.05 was taken as a statistically significant result.

3. Results

3.1 Phytochemical Profile of *Moringa oleifera* Extract

The *Moringa oleifera* leaf extract exhibited a wide range of phytochemicals including phenolic acids, flavonoids, tannins, terpenoids, and other bioactive components. The extraction yielded a concentrated plant extract, which could be used for further phytochemical and nanoparticle synthesis experiments. Preliminary phytochemical

Frontier in Medical & Health Research

ISSN: (e) 3007-1607 (p) 3007-1593

screening revealed the presence of phenolics, flavonoids, tannins, terpenoids, alkaloids and other secondary metabolites suggesting the possibility of the extract to be used as a biological reducing and stabilizing agent during the synthesis of silver nanoparticles. Total phenolics in the extract were 96.35 ± 4.21 mg of GAE/g of dry extract and the total flavonoids content was 48.72 ± 2.37 mg of QE/g of dry extract (Table 1). The results showed that there were significant amounts of phenolic and flavonoid compounds in the extract. The extract also showed antioxidant activity in both DPPH and ABTS assays which was concentration dependent. The DPPH radical-scavenging activity was found to be progressively increasing with the increase in concentration of the extract, reaching about 98% at 1600 µg/mL with estimated IC_{50} value of 74.38 µg/m*L*. Likewise, ABTS radical-scavenging activity rose with the concentration and reached a level of 99% at the highest concentration tested; the estimated IC_{50} was 58.91 µg/m*L*. The dose-response models had high goodness of fit, R2 values of 0.992 and 0.995 for DPPH and ABTS respectively (Figure 1E-F).

The phytochemical components of the extract were further confirmed by LC-MS/MS analysis (Figure 1A) which showed the presence of several major phytochemical constituents. The prominent signals of the representative chromatographic profile were assigned to gallic acid, chlorogenic acid, quercetin-3-O-glucoside, caffeic acid, rutin, kaempferol-3-O-glucoside, ferulic acid, apigenin and luteolin. Flavonoids (43.2%) were the most abundant phytochemical class followed by phenolic acids (28.7%), tannins (12.6%), terpenoids (8.9%), and other phytochemicals (6.6%) (Figure 1B). These chemically varied compounds offer a potential phytochemical explanation of reducing and capping activity of the extract in the synthesis of AgNPs.

Overall, the phytochemical and antioxidant analyses confirmed that the extract from *M. oleifera* shows high content of phenolic and flavonoids compounds and had high free-radical-scavenging properties, suggesting that *M. oleifera* extract was a suitable biological reagent for the green synthesis of AgNPs.

Table 1. Phytochemical composition, total phenolic and flavonoid contents, and antioxidant activity of *Moringa oleifera* leaf extract.

Parameter	Result
Extraction yield	18.6 ± 1.24% (w/w)
Phenolics	Detected
Flavonoids	Detected
Tannins	Detected
Terpenoids	Detected
Alkaloids	Detected
Total phenolic content	96.35 ± 4.21 mg GAE/g
Total flavonoid content	48.72 ± 2.37 mg QE/g
DPPH IC_{50}	74.38 µg/mL
DPPH R^2	0.992
ABTS IC_{50}	58.91 µg/mL
ABTS R^2	0.995

Values are presented as mean ± SD where applicable. GAE, gallic acid equivalents; QE, quercetin equivalents; IC_{50}, concentration producing 50% radical-scavenging activity.

Volume 4, Issue 3, 2026

Frontier in Medical & Health Research

ISSN: (e) 3007-1607 (p) 3007-1593

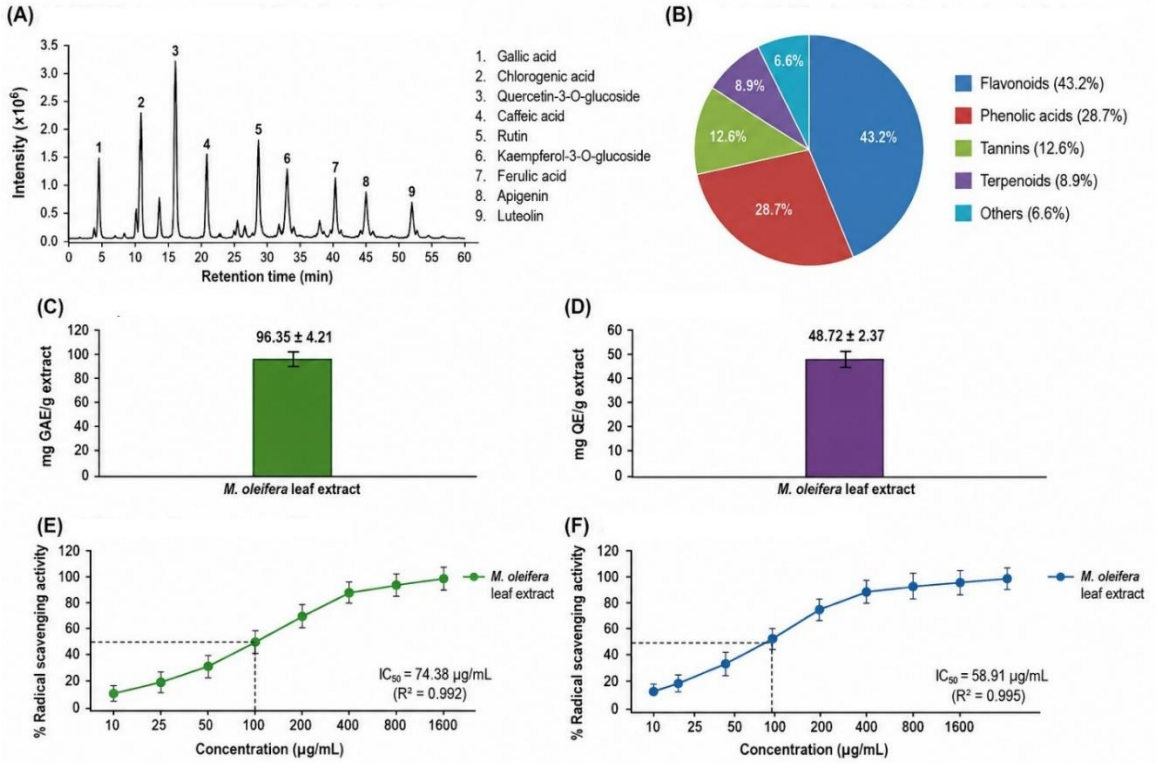


Figure 1. Phytochemicals and LC-MS/MS chromatographic profile of *Moringa oleifera* leaf extract. (A) Representative LC-MS/MS chromatogram of the detected major constituents such as gallic acid, chlorogenic acid, quercetin-3-O-glucoside, caffeic acid, rutin, kaempferol-3-O-glucoside, ferulic acid, apigenin, and luteolin. Relative percentage of the phytochemical classes found, flavonoids being the major class followed by phenolic acids, tannins, terpenoids and other phytochemicals. (C) Total phenolic content of the extract (mg GAE/g dry extract). (D) Total flavonoid content in terms of mg QE/g dry extract. (E) DPPH radical-scavenging activity) estimated IC_{50} value of 74.38 µg/m*L*. Concentration-dependent ABTS radical-scavenging activity with an estimated IC_{50} of 58.91 µg/mL (F). Data are shown as mean ± SD from independent experiments and nonlinear dose-response regression was used to calculate IC_{50} values.

3.2 Green Synthesis and Optimization of AgNPs

It was initially confirmed by a progressive visual color change of the reaction mixture from pale yellow to dark brown as the reaction mixture was kept for incubation, which shows that the color change is due to the reduction of Ag^+ ions to silver nanoparticles (AgNPs) (Figure 2B). The intensity of the brown colour increased with the reaction time and was found to be relatively constant after about 60 minutes, indicating that the formation of nanoparticles was fairly complete under the optimized conditions. The formation of AgNP was also confirmed by UV–Visible spectroscopic monitoring by the emergence of a characteristic surface plasmon resonance (SPR) band at ~ 420 nm (Figure 2C). The absorbance values rose along with the reaction time, and the SPR band rose also with the reaction time, suggesting that there was continual formation of nanoparticles. During the first few minutes of the reaction the absorption intensity at 420 nm increased rapidly and then reached a plateau after about 60-80 min, suggesting stabilization of the synthesis process (Figure 2H).

The formation of nanoparticles was significantly affected by the amount of $AgNO_3$ (Figure 2D). An increase in the precursor concentration caused a progressive increase in absorbance at 420 nm, up to 3 mM, while an increase to 5 and 10 mM lead to a decrease in absorbance, indicating that at higher precursor concentrations the formation of nanoparticles was less favourable and/or there was

Frontier in Medical & Health Research

ISSN: (e) 3007-1607 (p) 3007-1593

increased aggregation. The λmax of the nanoparticles was consistent at various concentrations, about 410–430 nm. Likewise, the concentration of the *M. oleifera* extract had significant effect on the formation of nanoparticles (Figure 2E). Increasing extract concentration was directly related to increasing absorbance until about 2 mg/mL, where no significant change was noticed. As the concentration of the extract increased, the absorbance of the nanoparticles slightly decreased, indicating that the excess amount of phytochemicals may affect the nucleation and/or the colloidal properties of the nanoparticles. The maximum of the SPR was kept fairly constant at 420 nm. The pH of the reaction also had an effect on the formation of AgNP (Figure 2F). The absorbance of SPR increased with the increase of pH from 4 to about 8. Absorbance went down at higher pH (above 8), which means that very alkaline conditions were not the best for the optimized synthesis. The relatively constant λmax over the range of pH tested indicated that the main pH effect was on the efficiency of nanoparticle formation, and optical parameters of the particles did not change significantly.

The temperature-dependent analysis showed that the formation of nanoparticles was favored at higher reaction temperature, ranging from 20°C until the temperature reaches around 40°C (Figure 2G). The absorbance maximum was found at 40°C, and on increasing further the temperature the absorbance gradually decreased. These results suggested that 40°C was the optimal temperature for both high rates and reproducible formation of the AgNPs with reduced potential temperature complications. The optimized condition of 3 mM $AgNO_3$, 2 mg/mL *M. oleifera* extract, pH 8 and 40°C allowed for the rapid development of the SPR band, which achieved a stable profile after about 60 min (Figure 2H). The absorbance at 420 nm rose significantly up to 60 min and then leveled off up to 120 min. During the monitoring period, the λmax stayed around 420 nm and the absorbance at 700 nm was low, suggesting that there was little aggregation. Thus, the optimum synthesis conditions for further physicochemical characterization and biological tests were: 3 mM $AgNO_3$, 2 mg/mL extract, pH 8, 40°C, and 60 min.

Volume 4, Issue 3, 2026

Frontier in Medical & Health Research

ISSN: (e) 3007-1607 (p) 3007-1593

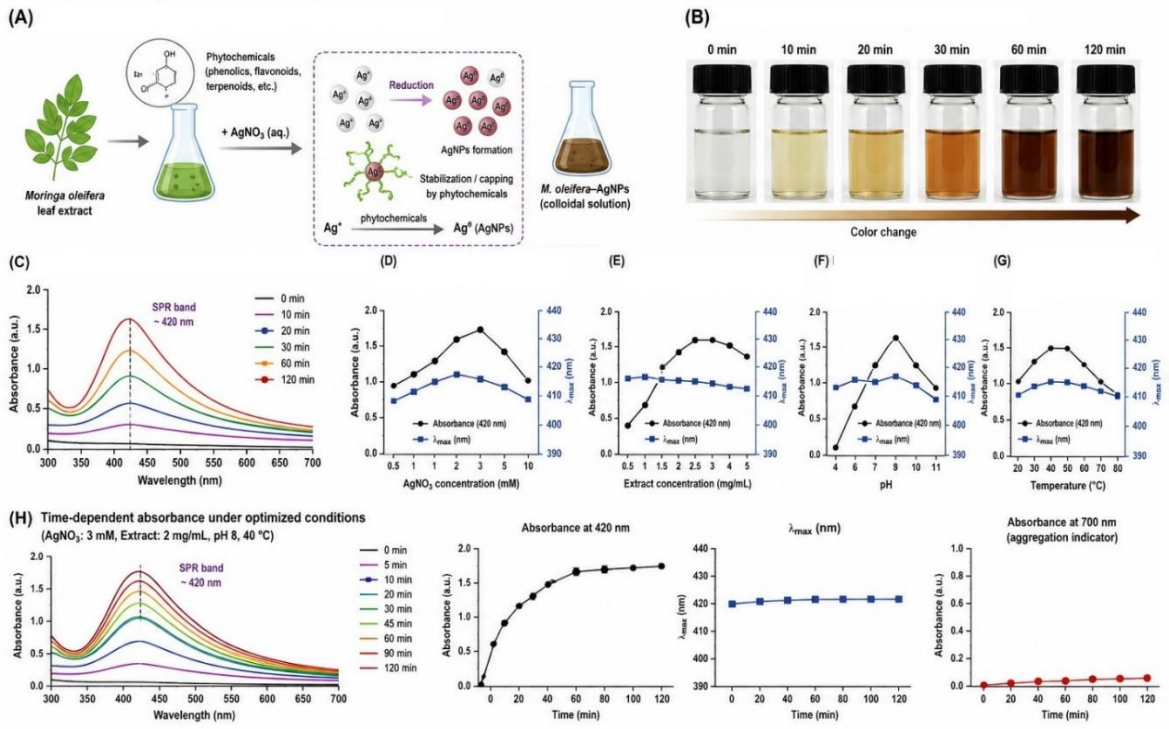


Figure 2. Optimization and monitoring procedure of green synthesis of silver nanoparticles using *Moringa oleifera* (Mora). Schematic representation of phytochemicals mediated reduction of Ag+ and formation of AgNP in *M. oleifera* extract, followed by the stabilization/capping of the nanoparticles. Representative colour changes in the reaction mixture in (B) and development of the SPR band at ~ 420 nm in the UV–Visible spectra in (C) as a function of reaction time. Absorbance (optical density) at 420 nm and λmax of $AgNo_3$ solution as a function of its concentration. (E) *M. oleifera* extract concentration effect on the formation of AgNP. (F) Influence of reaction pH on the formation of nanoparticles. Effect of reaction temperature on SPR intensity (G). Time-dependent nanoparticles formation under optimized condition with absorbance at 420 nm, λmax stability, and low absorbance at 700 nm as an indication of low aggregation. The optimized parameters for the synthesis were 3 mM of $AgNO_3$, 2 mg/mL of the extract, pH 8, temperature 40°C and reaction time of 60 min.

3.3 Physicochemical Characterization and Stability of AgNPs

The optimized *Moringa oleifera* mediated silver nanoparticles (AgNPs) showed different physicochemical properties which indicated successful formation of nanoparticles, crystalline metallic silver composition, mostly spherical morphology and good colloidal stability (Table 2 and Figure 3). The surface plasmon resonance band was observed in the UV–Visible spectroscopy and was centered around 420 nm, which is expected for the formation of nanoscale silver (Figure 3A). A relatively narrow and symmetrical SPR profile meant that there was a comparatively homogeneous population of nanoparticles, and little aggregation. FTIR analysis of *M. oleifera* extract revealed several characteristic absorptions such as at 3370, 2924, 1631, 1384 and 1054 cm-1. After AgNP synthesis, these bands were slightly changed to 3352, 2921, 1628, 1381, and 1051 cm^{-1}, respectively (Figure 3B). The changes imply the participation of hydroxyl, carbonyl, C–O and other phytochemical functional groups in the reduction and stabilizing of the silver ions on the surface of the nanoparticles.

Frontier in Medical & Health Research

ISSN: (e) 3007-1607 (p) 3007-1593

The XRD pattern shows characteristic diffraction peaks at 38.1°, 44.3°, 64.5°, and 77.4° that correspond to crystallographic plane (111), (200), (220), and (311) of face-centered cubic metallic silver, respectively (Figure 3C). There was no indication of significant additional crystalline phases, which would indicate the presence of mostly crystalline AgNPs. There were mainly spherical to quasi-spherical in shape and relatively uniformly distributed SEM analysis of synthesized nanoparticles showed some clustering of the nanoparticles was evident in localized areas (Figure 3D). The TEM image further revealed that the particles have a predominantly spherical shape, with an average primary particle diameter of 18.6 ± 6.4 nm derived from 200 individual nanoparticles (Figure 3E-F). Most of the particles were located in the range of ~10 to 50 nm, and there were relatively few particles larger than 100 nm. Elemental analysis by EDX analysis showed that the analyzed material contained about 71.45 wt% and 40.27 at% of the element silver (Figure 3G). A few additional signals were also identified: carbon signals (aprox. 11.21 wt%) and oxygen signals (aprox. 17.34 wt%), which were due to plant-derived organic compounds related to the surface of the nanoparticles.

The hydrodynamic diameter from the DLS analysis was 22.8 nm with a peak diameter of ~ 21.3 nm and PDI of 0.184 (Figure 3H). This difference in the hydrodynamic diameter from the TEM primary particle size was consistent with the presence of a hydrated layer of the phytochemical that caps the metallic nanoparticle core. The PDI of the relatively low value suggested a relatively narrow particle-size distribution. The synthesized AgNPs had a zeta potential of about −28.7 mV (Figure 3I), which is indicative of a negative surface charge on the synthesized nanoparticles and is a good electrostatic stabilization of the colloidal suspension. The hydrodynamic particle size was found to be fairly stable, and did not show significant changes throughout the period of stability assessment. Likewise, minimal changes were observed in PDI and zeta potential, but there was a relatively stable absorbance of the SPR (Figure 3J). These results suggest that the optimized formulation of AgNP retained its colloidal properties and there was negligible evidence of significant aggregation during storage. The independent synthesis batches also showed similar particle size, PDI, zeta potential and SPR, with a good batch-to-batch reproducibility of the optimized green-synthesis procedure. In general, the physicochemical analyses showed successful synthesis of nanocrystalline silver particles that are primarily spherical in shape, produced with a surface that is linked to phytochemicals, and have good colloidal stability.

Table 2. Physicochemical characteristics and stability parameters of *Moringa oleifera*-AgNPs.

Parameter	Characteristic/Result
SPR λmax	420 nm
TEM primary particle size	18.6 ± 6.4 nm
Number of particles analyzed by TEM	200
DLS hydrodynamic diameter	22.8 nm
DLS peak size	21.3 nm
Polydispersity index (PDI)	0.184
Zeta potential	−28.7 mV
XRD peak 1	38.1° (111)
XRD peak 2	44.3° (200)
XRD peak 3	64.5° (220)
XRD peak 4	77.4° (311)
Crystalline phase	Face-centered cubic metallic Ag
Ag content by EDX	71.45 wt%
Ag atomic percentage	40.27%

Frontier in Medical & Health Research

ISSN: (e) 3007-1607 (p) 3007-1593

Carbon by EDX	11.21 wt%
Oxygen by EDX	17.34 wt%
Major FTIR bands — extract	3370, 2924, 1631, 1384, 1054 cm^{-1}
Major FTIR bands — AgNPs	3352, 2921, 1628, 1381, 1051 cm^{-1}
Stability assessment	Stable with minor variation
Storage condition shown in Figure 3	4°C
Stability monitoring period	91 days
Batch reproducibility	Comparable physicochemical profiles

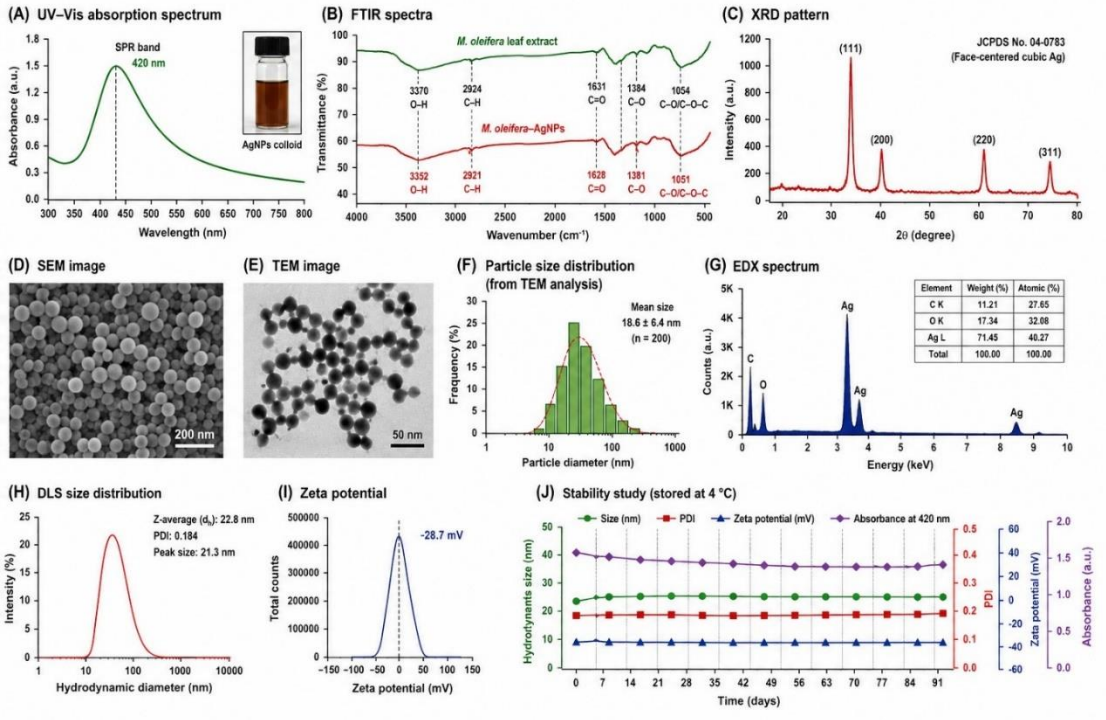


Figure 3. Characterization and stability study of green-synthesized *Moringa oleifera*-AgNPs. (A) Absorption spectrum of UV–Visible light with a characteristic SPR band at around 420 nm. Note that minor changes in the characteristic bands of hydroxyl, C–H, carbonyl, C–O, and related functional groups are observed in the FTIR spectra of *M. oleifera* extract and synthesized AgNPs after the formation of nanoparticles. The XRD pattern (C) contains the peaks of face centered cubic metallic silver structure at 38.1°, 44.3°, 64.5°, and 77.4°, which correspond to the (111), (200), (220), and (311) planes of the face centered cubic metallic silver structure, respectively. (D) Representative SEM image indicating the presence of mostly spherical shaped nanoparticles with relatively uniform distribution. (E) TEM image showing nanoscale spherical particles. The particle-size distribution obtained by TEM analysis of 200 single nanoparticles with a mean particle size of 18.6 ± 6.4 nm (F). (G) EDX spectrum confirming the presence of silver as the main component detected, along with carbon and oxygen, which are elemental components of the surface matrix of plants. The DLS particle-size distribution of this sample has a hydrodynamic diameter of 22.8 nm, a peak size of 21.3 nm and a PDI of 0.184. (I) Zeta-potential distribution with a surface charge of −28.7 mV. In terms of (J) stability profile during storage at 4°C, relatively small variation in hydrodynamic size, PDI and ζ-potential were observed over the period of monitoring (91 days) as were small variation in absorbance at 420 nm. The images with the SEM and TEM were marked with scale bars.

Frontier in Medical & Health Research

ISSN: (e) 3007-1607 (p) 3007-1593

3.4 Antileishmanial Activity Against *L. major* Promastigotes

Moringa oleifera-AgNPs showed a time and concentration-dependent antileishmanial activity against promastigotes of Leishmania major (Figure 4). The viability of the parasites decreased with increasing concentration of AgNP, from 96.8 ± 3.2% at 1 µg/mL to 8.3 ± 2.4% at 400 µg/mL (Figure 4A). The parasite growth inhibition also showed to be concentration-dependent, ranging from 3.2 ± 1.1% at 1 µg/mL to 91.7 ± 3.6% at 400 µg/mL (Figure 4B). It was found that AgNP treatment had a strong concentration-response relationship (higher R^2 value of 0.987; Figure 4C; Table 3) with an estimated IC_{50} value of 44.7 µg/mL and an IC_{90} value of 182.5 µg/m*L*. The results show that the green synthesized AgNPs could successfully inhibit the viability of the parasites under relatively low concentration. Exposure time was also found to affect the antileishmanial effect (Figure 4D). At the AgNP IC_{50} concentration of 44.7 µg/mL, parasite viability decreased from 100.0 ± 4.1% at baseline to 93.2 ± 3.7% at 6 h, 82.4 ± 4.2% at 12 h, 61.3 ± 3.9% at 24 h, 35.8 ± 3.1% at 48 h, 22.6 ± 2.7% at 72 h, and 14.7 ± 2.3% at 96 h. As the exposure time increased, the proportion of parasites that were inhibited increased, with the highest proportions of inhibition found after 72-96 hours. Comparative analysis revealed that the *M. oleifera*-AgNPs had significantly higher anti-leishmanial activity compared to the plant extract and $AgNO_3$ alone in the range of the tested concentrations (Figure 4E). AgNPs exhibited around 88% inhibition, while $AgNO_3$ and *M. oleifera* extract showed around 70% and 48% inhibition, respectively, at 200 µg/m*L*. The best inhibitions were observed with the reference drug miltefosine over the concentration range with maximum inhibition of ~ 100 µg/mL at 200 µg/m*L*. The IC_{50} and IC_{90} also showed the relative potency of the treatments (Figure 4F; Table 3). The synthesize AgNPs (44.7 µg/mL) had an IC_{50} value that was about four times lower than the IC_{50} of $AgNO_3$ (96.3 µg/mL) and was about four times lower than the IC_{50} of the *M. oleifera* extract (183.2 µg/mL). Similarly, the AgNP IC_{90} (182.5 µg/mL) was lower than those of $AgNO_3$ (297.6 µg/mL) and the plant extract (682.7 µg/mL). Miltefosine had the highest potency with an IC_{50} of 7.8 µg/mL and an IC_{90} of 28.3 µg/m*L*. The findings showed that green-synthesized *M. oleifera*-AgNPs have significantly higher promastigote inhibitory activity than *M. oleifera* extract and $AgNO_3$ under the tested conditions with *M. oleifera*-AgNPs still showing potential as promastigote inhibitors, albeit less potent than the reference antileishmanial drug.

Table 3. IC_{50} and IC_{90} values of *M. oleifera*-AgNPs, *M. oleifera* extract, $AgNO_3$, and reference drug against *L. major* promastigotes.

Treatment	IC_{50} (µg/mL)	IC_{90} (µg/mL)	Relative potency based on IC_{50}
***M. oleifera* extract**	183.2	682.7	Lowest among experimental treatments
$AgNO_3$	96.3	297.6	Moderate
***M. oleifera*-AgNPs**	**44.7**	**182.5**	**Highest among experimental treatments**
Miltefosine	**7.8**	**28.3**	**Highest overall**

Volume 4, Issue 3, 2026

Frontier in Medical & Health Research

ISSN: (e) 3007-1607 (p) 3007-1593

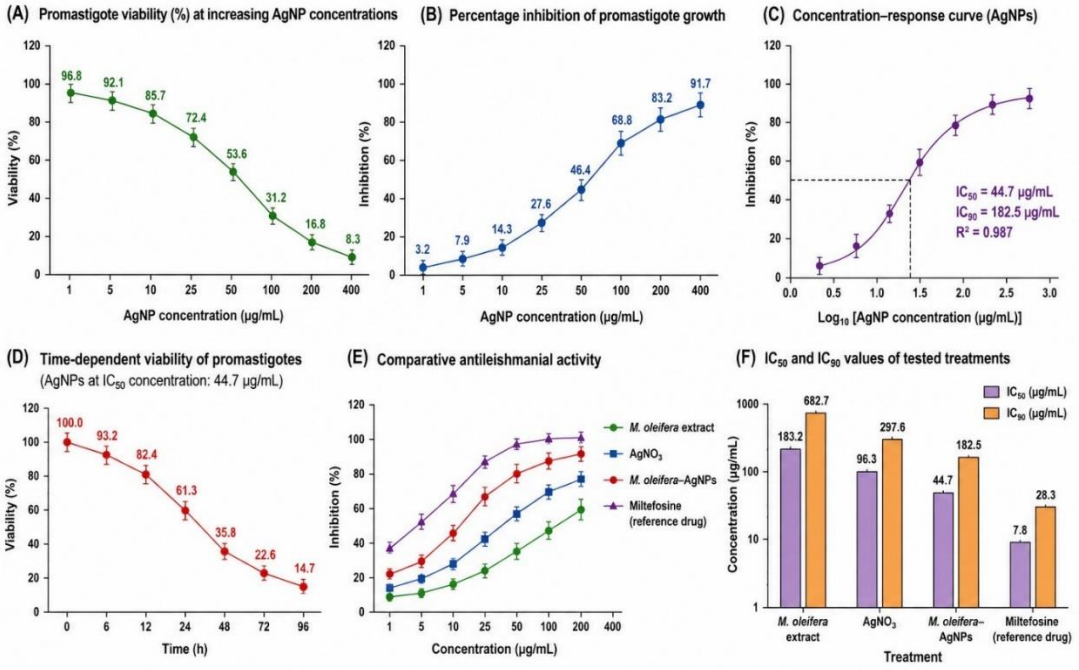


Figure 4. Concentration- and time-dependent antileishmanial activity of green-synthesized *M. oleifera*-AgNPs against Leishmania major promastigotes. (A) Reduction in viability of promastigotes after exposure to 1–400 µg/mL AgNPs, which was concentration dependent. Parasite-growth inhibition (B) is proportionate to the change in concentration. The concentration-response curve is (C) which has an estimated IC_{50} of 44.7 µg/mL and an IC_{90} of 182.5 µg/mL (R^2 = 0.987). Time-dependent decrease in parasite viability after exposure to AgNPs at the IC_{50} concentration (44.7 µg/mL) which shows progressive loss of viability from 0 to 96 h. Comparative concentration-response profile of *M. oleifera* extract, $AgNO_3$, green synthesized *M. oleifera*-AgNPs and Miltefosine. (F) Comparison of IC_{50} and IC_{90} values of the different treatments used. Data are given as mean ± SD (three independent experiments, triplicate). IC_{50} and IC_{90} values were estimated using nonlinear dose-response regression.

3.5 Activity Against Intracellular *L.* major Amastigotes

The green synthesized *Moringa oleifera*-AgNPs showed strong activity to the intracellular Leishmania major amastigotes, which was confirmed by the reduction of the macrophage infection, the parasite burden inside the macrophage and the infection index (Table 4; Figure 5). A high intracellular parasite burden in untreated infected macrophage cells was observed, while treatment with *M. oleifera* extract, AgNPs and miltefosine gradually decreased the amastigotes inside the cells (Figure 5A). The proportion infection of the untreated infected control was 86.7 ± 6.0%. This was reduced to 58.4 ± 7.8% with *M. oleifera* extract and 33.6 ± 5.2% at 12.5 µg/mL and 17.2 ± 3.4% at 25 µg/mL for AgNP treatment (Figure 5B). The reference drug, miltefosine (10 µg/mL) gave the lowest percentage of infected macrophages (8.6 ± 2.5%). The infection rates of all active treatments were significantly lower than the untreated infected control ($P < 0.001$). The same trend was seen for the level of intracellular parasite (ICP) (Figure 5C). The average number of amastigotes per infected macrophage in untreated infected macrophages was 50.1 ± 2.4 amastigotes per infected macrophage. This burden was reduced to 27.6 ± 2.1 after being treated with *M. oleifera* extract, and to 14.8 ± 1.6 and 6.2 ± 1.2 amastigotes/macrophage after treatment with 12.5 and 25 µg/mL AgNPs, respectively. Miltefosine was found to leave the lowest number of amastigotes, 2.4 ± 0.8 amastigotes/macrophage,

Frontier in Medical & Health Research

ISSN: (e) 3007-1607 (p) 3007-1593

in infected macrophages. The calculated infection index for untreated infected macrophages was 43.4 ± 2.5 and reduced to 16.1 ± 1.8 after treated with the plant extract (Figure 5D). AgNP treatment further reduced the infection index to 5.0 ± 0.9 at 12.5 µg/mL and 1.1 ± 0.4 at 25 µg/mL. The next lowest infection index (0.2 ± 0.1) was observed in the reference drug, suggesting near complete suppression of intracellular infection under the tested conditions. The M. *oleifera* extract showed relative reduction in intracellular parasite burden of 62.9%, AgNPs at 12.5 and 25 µg/mL showed 80.4% and 94.7% reduction respectively when compared to untreated infected control (Figure 5E). A 99.5% reduction was obtained with Miltefosine. This makes the green synthesized AgNPs as a significant dose-dependent reduction in the intracellular parasite burden with significantly higher activity than the plant extract itself. Concentration-response analysis also showed that there was a good correlation between AgNP concentration and the inhibition of intracellular amastigotes (Figure 5F). A goodness-of-fit of $R^2 = 0.985$ was achieved when a nonlinear dose-response regression was performed with an estimated IC_{50} of 12.1 µg/mL and an IC_{90} of 36.3 µg/mL. These values were much lower than those seen in the promastigote stage, suggesting a significant effect of the AgNP formulation against the intracellular parasite stage.

Table 4. Effects of *Moringa oleifera*-AgNPs and comparator treatments on intracellular *L. major* infection.

Treatment	Concentration (µg/mL)	Infected macrophages (%)	Amastigotes/macrophage	Infection index	Reduction in parasite burden (%)
Uninfected control		2.3 ± 0.8			
Untreated infected control	0	86.7 ± 6.0	50.1 ± 2.4	43.4 ± 2.5	0
***M. oleifera* extract**	200	58.4 ± 7.8	27.6 ± 2.1	16.1 ± 1.8	62.9
***M. oleifera*-AgNPs**	12.5	33.6 ± 5.2	14.8 ± 1.6	5.0 ± 0.9	80.4
***M. oleifera*-AgNPs**	25	17.2 ± 3.4	6.2 ± 1.2	1.1 ± 0.4	94.7
Miltefosine	10	8.6 ± 2.5	2.4 ± 0.8	0.2 ± 0.1	99.5

Volume 4, Issue 3, 2026

Frontier in Medical & Health Research

ISSN: (e) 3007-1607 (p) 3007-1593

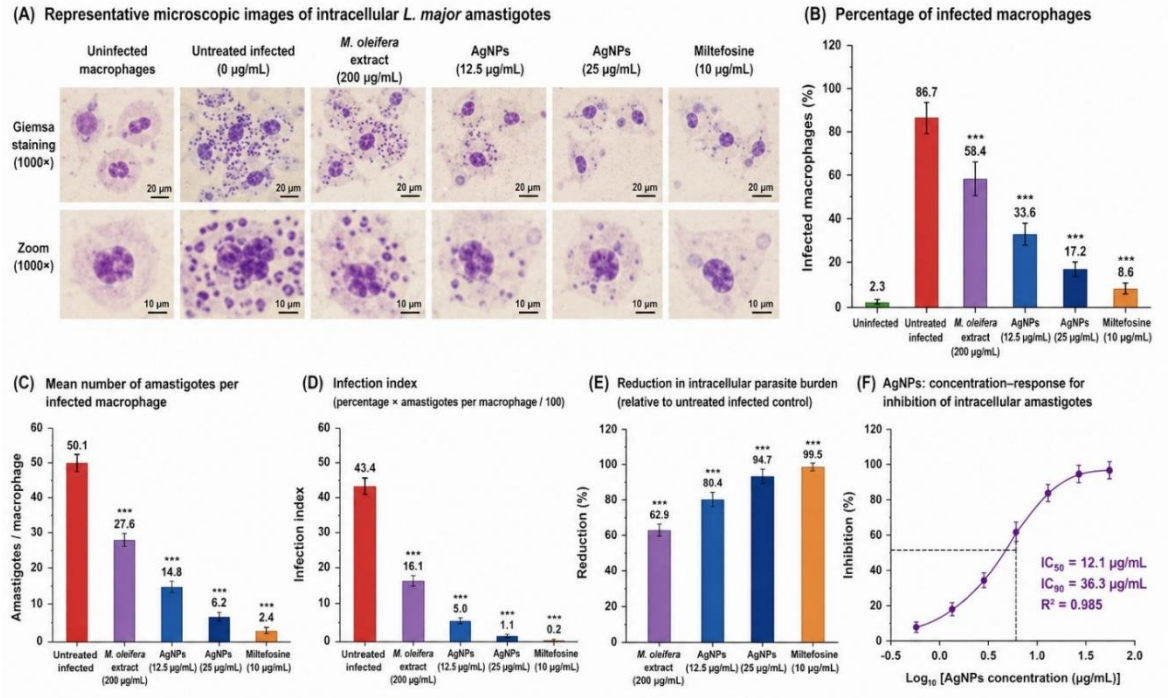


Figure 5. Inhibitory effect of *Moringa oleifera*-AgNPs on the intracellular amastigotes of Leishmania major. Representative Giemsa stained microscopic images of uninfected macrophages, uninfected macrophages treated with *M. oleifera* extract, AgNPs and infected macrophages treated with miltefosine. (B) Percentage of infected macrophages after treatment, which exhibited concentration-dependent reduction by AgNPs. (C) Average number of amastigotes in the interior of an infected macrophage. (D) Infection index as a percentage of macrophages infected and the amount of parasite in the cel*L.* (E) Percentage of decrease in intra cellular parasite load as compared to untreated infected contro*L.* Concentration-response curve for the intracellular amastigotes inhibited by the AgNP, with an estimated IC_{50} of 12.1 µg/mL and IC_{90} of 36.3 µg/mL (R^2 = 0.985). All data are given as mean ± SD from three separate experiments that were repeated three times. One-way ANOVA and Tukey's post-hoc test were used to determine statistical significance, with asterisk (P<0.001 versus the untreated infected control). Representative images were captured of the micro images under the same imaging conditions; Scale bars are shown.**

3.6 Cytotoxicity, Hemocompatibility, and Selectivity

The cytotoxicity and parasite selective activity of the tested treatments was assessed using mammalian cells as comparison, with the exception of M. *oleifera* extract, $AgNO_3$, green-synthesized AgNPs and miltefosine (Table 5; Figure 6). The treatments each exhibited concentration-dependent effects on mammalian-cell viability (Figure 6A). M. *oleifera* extract exhibited the least cell death with about 70% cell viability even at the highest concentration tested. Cell viability decreased progressively with the use of $AgNO_3$, M. *oleifera*-AgNPs, and miltefosine.The miltefosine had the most potent cytotoxic effect, followed by $AgNO_3$ and M. *oleifera*-AgNPs. Nonlinear dose-response analysis showed that CC_{50} for M. *oleifera* extract, $AgNO_3$, green-synthesized AgNPs and miltefosine were >1000 µg/mL, 412.6 µg/mL, 231.8 µg/mL, and 35.7 µg/mL, respectively (Figure 6B). The fitted models were found to be good with R^2 values between 0.972 and 0.985. However, despite their higher toxicity towards mammalian cells than crude plant extract, AgNPs had a considerably higher CC_{50} compared to their IC_{50} against *L.* donovani. The quantitative viability results (Figure 6C) agreed with the microscopic examination. Untreated

Frontier in Medical & Health Research

ISSN: (e) 3007-1607 (p) 3007-1593

mammalian cells had normal morphology that included proper cellular spreading and attachment. While exposure to *M. oleifera* extract caused relatively small morphological changes, $AgNO_3$ and AgNP induced concentration-dependent changes such as increased cellular rounding, decreased cell attachment, cellular shrinkage and other morphological alterations. The most significant morphological changes were noted after receiving miltefosine treatment. The hemocompatibility evaluation demonstrated low hemolytic activity of the green synthesized AgNPs in the concentration range used (Figure 6D). Hemolysis increased from 1.2% at 1 µg/mL to 35.4% at 400 µg/m*L*. Importantly, hemolysis was not above the set threshold of 5% up to around 10 µg/mL, with increasing concentrations increasing the level of hemolysis of the erythrocyte membranes. These results show a dose dependency for the hemolytic reaction.

The antileishmanial potency compared to the mammalian cell toxicity showed a clear separation of doses needed for parasite inhibition and mammalian cell toxicity (Figure 6E). The AgNP IC_{50} of promastigotes was 44.7 µg/mL, whereas the mammalian-cell CC_{50} was 231.8 µg/m*L*. The IC_{50} for intracellular amastigotes was much lower at 12.1 µg/m*L*. However, the IC_{50} values for $AgNO_3$ were 96.3 and 39.8 µg/mL for promastigotes and amastigotes, respectively, whereas those of *M. oleifera* extract were 183.2 µg/mL and 75.6 µg/mL for promastigotes and amastigotes, respectively. The calculated selectivity indexes also showed parasite selective activity of the treatments (Figure 6F). The SI values of AgNPs were 5.2 against promastigotes and 19.2 against intracellular amastigotes. The SI values of $AgNO_3$ and *M. oleifera* extract were 4.3 and >5.5, and 10.4 and >13.2 respectively. The SI of Miltefosine were 4.6 against promastigotes and 12.3 against amastigotes. The overall outcome of this study was the green-synthesized AgNPs that showed a good compromise between the ability to kill leishmanial cells and to be toxic to mammalian-cell culture, especially to the intracellular amastigotes of *L. major*. In comparison to the amastigote IC_{50}, the relatively high CC_{50} and SI of 19.2 at the conditions tested in the experiment suggested large therapeutic margin.

Table 5. Cytotoxicity, hemolysis, and selectivity indices of experimental treatments.

Treatment	CC_{50} (µg/mL)	IC_{50} Promastigotes (µg/mL)	IC_{50} Amastigotes (µg/mL)	SI Promastigotes	SI Amastigotes	Hemolysis*
***M. oleifera* extract**	>1000	183.2	75.6	>5.5	>13.2	
$AgNO_3$	412.6	96.3	39.8	4.3	10.4	
***M. oleifera*-AgNPs**	**231.8**	**44.7**	**12.1**	**5.2**	**19.2**	1.2–35.4%
Miltefosine	35.7	7.8	2.9	4.6	12.3	

*For AgNPs, hemolysis ranged from 1.2% at 1 µg/mL to 35.4% at 400 µg/m*L*. **SI = CC_{50}/IC_{50}.** CC_{50}, concentration causing 50% mammalian-cell cytotoxicity; IC_{50}, concentration causing 50% parasite inhibition; SI, selectivity index.

Volume 4, Issue 3, 2026

Frontier in Medical & Health Research

ISSN: (e) 3007-1607 (p) 3007-1593

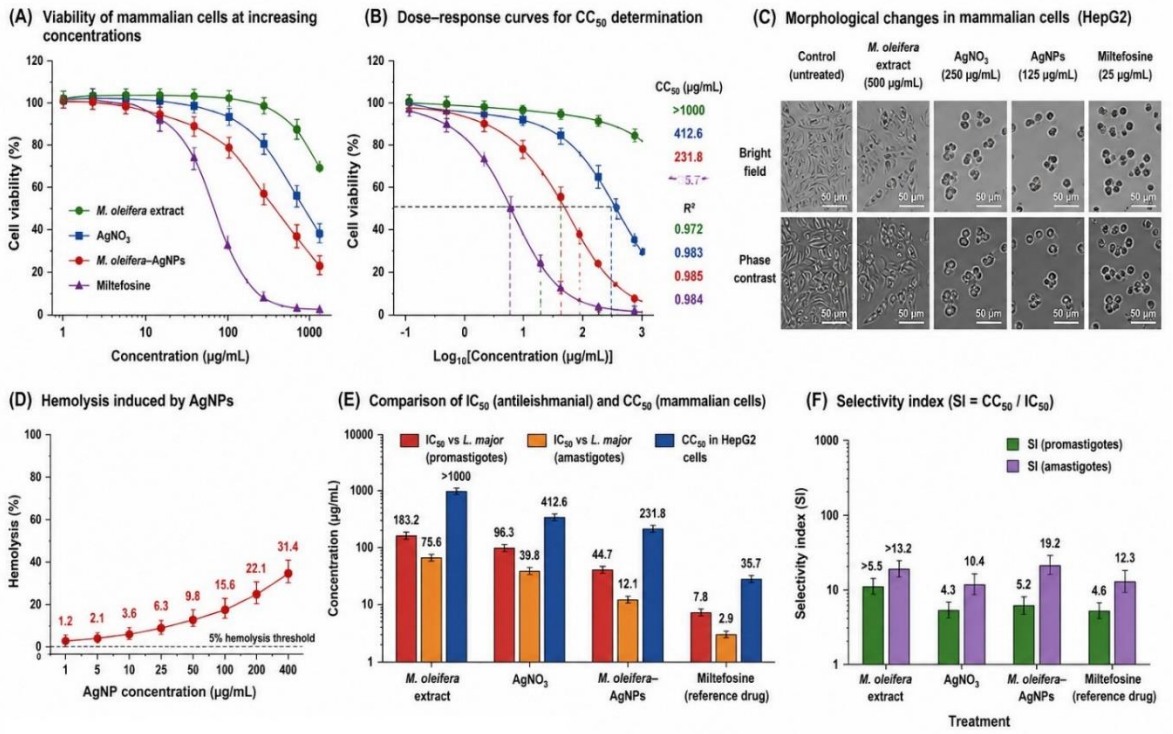


Figure 6. Green synthesized *Moringa oleifera*-AgNPs exhibits cytotoxic, hemocompatible and parasite selective activity. Concentration dependent viability of mammalian cells following exposure to *M. oleifera* extract, $AgNO_3$, green synthesized AgNPs and miltefosine. (B) CC_{50} values for the extract of *M. oleifera*, $AgNO_3$, AgNPs and miltefosine were estimated using nonlinear dose-response curves with CC_{50} values of >1000, 412.6, 231.8 and 35.7 µg/mL respectively. In (C), representative bright-field and phase-contrast images are shown to illustrate the morphological changes in mammalian cells observed through concentration. The dashed line indicates the 5% hemolysis threshold and the inset shows the effect of AgNPs on hemolysis as a function of concentration. Table showing IC_{50} values for antileishmanial activity compared to promastigotes and intracellular amastigotes and to mammalian-cell CC_{50} values. The selectivity indices (SI) calculated as CC_{50}/IC_{50} were 5.2 for promastigotes and 19.2 for intracellular amastigotes for AgNPs. All results are given as mean ± SD of three independent experiments, each done in triplicate.

3.7 Oxidative Stress and Mitochondrial Dysfunction.

The green synthesized *Moringa oleifera*-AgNPs had a significant concentration-dependent disruption of redox homeostasis and mitochondrial function in Leishmania major promastigotes (Table 6; Figure 7). The intracellular ROS levels were gradually elevated as AgNP concentrations were raised, whereas the antioxidant defenses, mitochondrial membrane potential, and ATP level in the cells were gradually decreased. AgNP induced a significant generation of intracellular ROS (Figure 7A–B). The proportion of ROS-positive parasites increased from 8.7 ± 1.8% in untreated parasites to 25.6 ± 3.0%, 51.3 ± 3.5%, and 82.6 ± 4.2% following treatment with 6.25, 12.5, and 25 µg/mL AgNPs, respectively. The enhanced increase was seen at all tested concentrations with maximum ROS being recorded at 25µg/mL ($P<0.001$). A dose-dependent decrease in reduced glutathione (GSH) was seen after the AgNP treatment (Figure 7C). GSH levels declined from 100% of control in untreated parasites to 72.4 ± 3.1%, 46.1 ± 3.8%, and 21.8 ± 2.6% at 6.25, 12.5, and 25 µg/mL, respectively. Therefore, the exposure of AgNPs at 25 µg/mL was correlated with about 78% reduction in GSH as compared with untreated

Frontier in Medical & Health Research

ISSN: (e) 3007-1607 (p) 3007-1593

parasites. Likewise, SOD and CAT activity was significantly decreased after nanoparticle exposure (Figure 7D–E). SOD activity decreased from 100% in untreated parasites to 78.6 ± 3.4%, 53.7 ± 3.1%, and 28.3 ± 2.7% at 6.25, 12.5, and 25 µg/mL, respectively. CAT activity showed a comparable pattern, declining to 74.3 ± 3.0%, 48.8 ± 3.5%, and 24.2 ± 2.4%, respectively. The results show that there is a significant suppression of the parasite antioxidant defense system at the dosages used. However, the MDA level was noticeably elevated due to AgNP treatment, indicating increased lipid peroxidation (Figure 7F). Relative to the untreated control, MDA increased to 142.3 ± 6.1% at 6.25 µg/mL, 188.6 ± 7.4% at 12.5 µg/mL, and 260.4 ± 8.2% at 25 µg/mL. The membrane lipid oxidations were clearly apparent at the highest concentration, where the increase was nearly 2.6-fold. Exposure to AgNP also resulted in significant mitochondrial dysfunction (Figure 7G). The ratio of red/Green fluorescence of JC-1 to untreated cells was 100%, 68.1 ± 4.0%, 40.2 ± 3.2% and 18.7 ± 2.1% at 6.25 µg/mL, 12.5 µg/mL, 25 µg/mL and 50 µg/mL, respectively. The JC-1 fluorescence profiles shown here are associated with a progressive transition from aggregated JC-1 signals to JC-1 monomolecular fluorescence, which is indicative of mitochondrial depolarization.

The corresponding decrease in cellular ATP was seen (Figure 7H). ATP levels decreased from 100% in untreated parasites to 73.4 ± 3.2%, 46.7 ± 3.5%, and 21.5 ± 2.4% following exposure to 6.25, 12.5, and 25 µg/mL AgNPs, respectively. As such, mitochondrial dysfunction was correlated with a significant decrease in energy availability of the cells. In addition, the production of Mitochondrial ROS was significantly increased in treated parasites (Figure 7I). MitoSOX fluorescence increased from 100% in untreated parasites to 168.7 ± 7.2%, 268.4 ± 9.1%, and 412.9 ± 12.4% at 6.25, 12.5, and 25 µg/mL, respectively. The mitochondrial oxidative stress was observed to be very high at 25µg/mL, which represents the roughly fourfold increase.

Table 6. Oxidative-stress and mitochondrial parameters following AgNP treatment.

Parameter	Control (0 µg/mL)	6.25 µg/mL	12.5 µg/mL	25 µg/mL
ROS-positive parasites (%)	8.7 ± 1.8	25.6 ± 3.0	51.3 ± 3.5	82.6 ± 4.2
GSH (% of control)	100.0 ± 3.2	72.4 ± 3.1	46.1 ± 3.8	21.8 ± 2.6
SOD activity (% of control)	100.0 ± 3.1	78.6 ± 3.4	53.7 ± 3.1	28.3 ± 2.7
CAT activity (% of control)	100.0 ± 3.0	74.3 ± 3.0	48.8 ± 3.5	24.2 ± 2.4
MDA (% of control)	100.0 ± 4.2	142.3 ± 6.1	188.6 ± 7.4	260.4 ± 8.2
Mitochondrial membrane potential (% of control)	100.0 ± 3.5	68.1 ± 4.0	40.2 ± 3.2	18.7 ± 2.1
ATP (% of control)	100.0 ± 3.4	73.4 ± 3.2	46.7 ± 3.5	21.5 ± 2.4
Mitochondrial ROS (% of control)	100.0 ± 4.1	168.7 ± 7.2	268.4 ± 9.1	412.9 ± 12.4

Values are presented as mean ± SD from three independent experiments performed in triplicate. GSH, reduced glutathione; SOD, superoxide dismutase; CAT, catalase; MDA, malondialdehyde; ROS, reactive oxygen species. Values expressed relative to untreated control where indicated.

Volume 4, Issue 3, 2026

Frontier in Medical & Health Research

ISSN: (e) 3007-1607 (p) 3007-1593

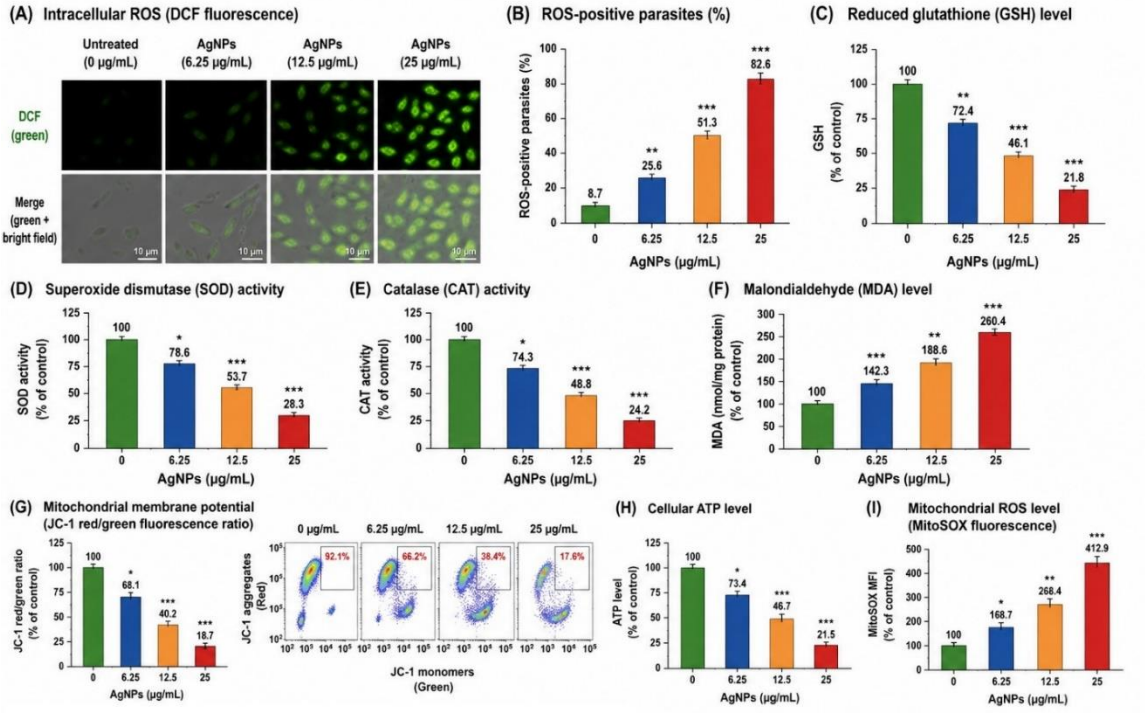


Figure 7. Role of AgNPs in generating oxidative stress and mitochondrial dysfunction in Leishmania major. (A) Representative DCF fluorescence images showing the generation of intracellular ROS in response to different concentrations of AgNPs (0, 6.25, 12.5, and 25 µg/mL). (B) Percentage of parasites positive for ROS (8.7% in untreated parasites and 82.6% at 25 µg/mL). The GSH level expressed as a percentage of the untreated control showing concentration dependent depletion (C). (D) Relative SOD activity of the treated sample. (E) CAT activity in relation to untreated controls. (F) MDA levels showing an increase in lipid peroxidation after exposure to AgNP. (G) Mitochondrial depolarization as determined by JC-1 as measured by the red/green fluorescence of JC-1, with progressive depolarization of the mitochondrial membrane, represented by JC-1 red/green fluorescence profiles and quantitative analysis. (EL) ATP levels relative to control (no treatment). Mitochondrial ROS measurement using MitoSOX fluorescence showing significant mitochondrial oxidative stress at increasing concentrations. The data are expressed as mean ± SD of three independent experiments, performed in triplicate. P < 0.05, *P < 0.01, and **P < 0.001 versus untreated control.

3.8 Cellular, Membrane and Ultrastructural changes

The green synthesize *Moringa oleifera*-AgNPs produced concentration dependent changes in the cellular, membrane, nuclear and ultrastructural levels of Leishmania major promastigotes (Table 7; Figure 8). These effects were manifested as progressive decrement in viability of parasites, higher percentage of apoptosis-like cells, damage to cell membrane, abnormalities in the nucleus, and marked ultrastructural damage. Annexin V/PI flow-cytometric analysis showed that the parasites transitioned from a viable population to early apoptosis-like, late apoptosis-like, and membrane-compromised population in a concentration-dependent manner (Figure 8A–B). In the untreated parasites, 92.8 ± 2.1% of the cells remained viable, while 3.3 ± 0.8% were found to have an early apoptosis-like phenotype, 2.3 ± 0.7% a late apoptosis-like phenotype and 1.6 ± 0.5% were membrane compromised. At 6.25 µg/mL AgNPs, viability declined to 76.6 ± 2.8%, accompanied by increases in early apoptosis-like (15.3 ± 1.9%), late apoptosis-like (6.2 ± 1.2%), and membrane-compromised (1.9 ± 0.6%) populations. When the concentration of parasites

Frontier in Medical & Health Research

ISSN: (e) 3007-1607 (p) 3007-1593

was increased to 12.5 µg/mL, the viable parasites were reduced further to 53.3 ± 2.5%, and the early and late apoptosis-like populations were raised to 28.3 ± 2.4% and 15.7 ± 1.8%, respectively. The viability of parasites decreased to 29.8 ± 2.7% at 25 µg/mL, whereas the number of parasites undergoing early apoptosis-like, late apoptosis-like and membrane-compromised increased to 35.0 ± 2.6%, 31.2 ± 2.3% and 4.0 ± 0.9%, respectively. The progressive nuclear abnormalities after AgNP exposure were also confirmed by fluorescence microscopy (Figure 8C). The untreated parasites had mainly stained and intact nuclei, which were uniformly stained. Nuclear fragmentation and chromatin condensation were correlated to the increase of the nanoparticle concentrations.Higher nanoparticle concentrations were correlated with condensed/fragmented nuclear structures and nuclear fragmentation. These observations were similar to the flow-cytometric evidence of apoptotic-like changes in cells. Membrane integrity analysis revealed a significant dose-dependent increase in membrane compromised parasites (Figure 8D). For example, the percentage of the SYTO 9-positive/PI-negative cells was reduced to 78.1%, 54.8%, and 29.7% when parasites were exposed to 6.25, 12.5, and 25 µg/mL AgNPs, respectively. In contrast, membrane-damaged parasites with PI were 21.9%, 45.2% and 70.3% in the treated, remodeled and modified samples, respectively. The progressive loss of membrane integrity suggested that at higher concentrations of nanoparticles significant disruption of the parasite plasma membrane had taken place. The surface morphological changes in AgNP-treated parasites were clearly observed using SEM analysis, showing parasites with different morphology compared to the relatively smooth and elongated morphology of the untreated parasites (Figure 8E). Parasites following treatment showed surface roughening, abnormal cell shape, membrane blebbing/protrusions and localized structural collapse. TEM also revealed significant changes within the cytoplasm at 25 µg/mL AgNPs, such as the presence of vacuolization, abnormal mitochondria, altered kinetoplast and nuclear changes (Figure 8F–H). The TEM-EDX analysis verified the presence of parasites associated with silver after AgNP exposure (Figure 8I). The EDX spectrum showed a strong peak for silver with the elemental profile of the sample indicating 62.62 wt% and 31.51 at% for silver. Carbon and oxygen were also identified, and the signals from copper were found to be due to the supporting grid/substrate. The presence of silver inside parasite associated structures supported the interaction and/or deposition of AgNP silver in treated parasites.

Table 7. Cellular and ultrastructural alterations induced by *M. oleifera*-AgNP treatment in *L. major*.

Parameter	Control	6.25 µg/mL	12.5 µg/mL	25 µg/mL
Viable parasites (%)	92.8 ± 2.1	76.6 ± 2.8	53.3 ± 2.5	29.8 ± 2.7
Early apoptosis-like (%)	3.3 ± 0.8	15.3 ± 1.9	28.3 ± 2.4	35.0 ± 2.6
Late apoptosis-like (%)	2.3 ± 0.7	6.2 ± 1.2	15.7 ± 1.8	31.2 ± 2.3
Membrane-compromised (%)	1.6 ± 0.5	1.9 ± 0.6	2.7 ± 0.7	4.0 ± 0.9
Membrane-intact cells (%)	93.6	78.1	54.8	29.7
PI-positive cells (%)	6.4	21.9	45.2	70.3
Nuclear morphology	Normal	Chromatin condensation	Nuclear fragmentation	Condensed/fragmented nuclei
Surface morphology	Normal	Mild alteration	Marked alteration	Severe disruption

Frontier in Medical & Health Research

ISSN: (e) 3007-1607 (p) 3007-1593

Cytoplasmic organization	Normal	Mild changes	Vacuolization	Pronounced disorganization
Mitochondrial morphology	Normal	Mild alteration	Swelling/structural alteration	Pronounced disruption
Silver localization	Not detected			Detected
Ag by TEM-EDX (wt%)				62.62
Ag by TEM-EDX (atomic%)				31.51

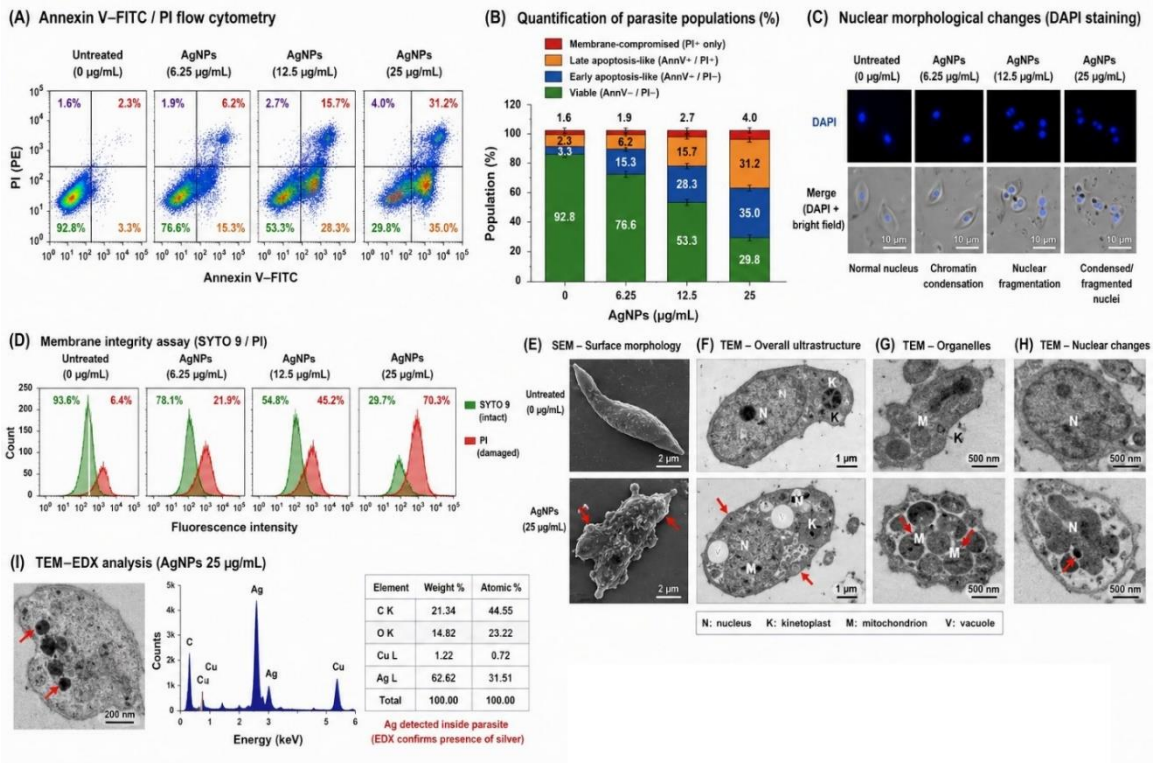


Figure 8. Changes in the cellular, membrane and ultrastructure of Leishmania major induced by *Moringa oleifera*-AgNPs synthesized by greening. Concentration-dependent redistribution of parasites from viable to apoptosis-like, and membrane-compromised populations was shown by (A) representative Annexin V-FITC/PI flow-cytometric plots. Exposure of 0, 6.25, 12.5, and 25 µg/mL AgNPs for quantification of the viable, early apoptosis-like, late apoptosis-like and membrane-compromised parasite population. (C) Representative DAPI stained fluorescent images showing the normal nucleus in untreated parasites and progressive condensation of chromatin, nuclear fragmentation, and condensed/fragmented nucleus after exposure to AgNP. (D) SYTO 9/PI staining of the membrane integrity, showing the shift towards an increasing number of membrane-damaged parasites (PI-fluorescence) in a concentration-dependent manner. (E) SEM images depicting the changes in surface morphology after AgNP treatment such as irregular morphology, surface disruption and structural collapse. (F) TEM images of changes in the overall ultrastructure inside the cells. TEM images (Higher) of mitochondrial and cytoplasmic abnormalities. (H) TEM images showing Treatment-induced Nuclear changes. They concluded that parasite-associated silver was present by (I) representative TEM-EDX analysis of AgNP-treated parasites with a characteristic silver

Frontier in Medical & Health Research

ISSN: (e) 3007-1607 (p) 3007-1593

signa*L.* Scale bars: (C) 10 µm; (E) 2 µm; (F) 1 µm; (G–H) 500 nm; (I) 200 nm. The results are given in the form of mean ± SD of three independent experiments, unless otherwise indicated.

3.9 Molecular Responses to AgNP Treatment

Leishmania major showed significant concentration-dependent gene expression alterations in oxidative stress, antioxidant defense, mitochondrial function, cellular stress, membrane homeostasis and programmed cell death after treatment with the green-synthesized *Moringa oleifera*-AgNPs (Table 8; Figure 9). As the concentration of the AgNP increased, the changes in gene expressions increased as well, especially at 12.5 and 25 µg/m*L*.

Oxidative-stress-related genes

On the other hand, treatment with AgNP resulted in a significant increase of oxidative-stress associated genes (Figure 9A). The relative expression for LmNOS2, LmNOX, LmTRX, LmPRX and LmGPX were increased by about 14.2-, 9.1-, 7.2-, 3.1- and 7.0-fold, respectively, when compared with the expression in untreated parasites at 25 µg/m*L*. This was a concentration dependent effect and already clear for several genes at concentrations of 6.25µg/m*L*. The highest induction was seen for LmNOS2, suggesting a strong induced transcription response to oxidative stress induced by AgNP.

Antioxidant-defense genes

However, genes related to antioxidant defense were progressively downregulated after AgNP exposure as compared to oxidative stress genes (Figure 9B). At 25 µg/mL, expression of LmSOD, LmCAT, LmGSH1, LmGR, and LmTR decreased to approximately 0.34-, 0.35-, 0.35-, 0.36-, and 0.28-fold, respectively. The transcriptional changes were in line with the biochemical results indicating decreases in SOD, CAT, and GSH following the exposure to the nanoparticles.

Mitochondrial and cellular stress-response genes

Genes involved in mitochondrial function and cell stress responses (Figure 9C) were also affected by AgNP treatment. The LmCYTb, LmND7, LmHSP70, LmHSP83, and LmATF4 were found to be up-regulated along the increasing concentration of AgNP. At 25 µg/mL, their expression was around 0.30-, 0.32-, 5.9-, 6.4- and 6.9-fold of that of the untreated parasites, respectively. Significant induction of heat-shock and stress-response genes was observed, suggesting high levels of cellular stress after AgNP exposure.

Membrane-homeostasis and cell-death-related genes

A significant change in the transcription of genes involved in membrane homeostasis and programmed cell death was also detected (Figure 9D). LmMDR1 and LmAQP1 decreased with increasing concentrations, with expression levels of ~0.35- and ~0.31-fold, respectively, at 25µg/m*L*. LmCasp-like and LmAIF, on the other hand, were gradually induced, with levels of about 3.5 and 8.3 times higher at the highest AgNP concentration, respectively.LmPS, LmCasp-like and LmAIF, in contrast, were gradually induced, with a level of 3.5-fold, 5.4-fold and 8.3-fold, respectively, at the highest AgNP concentration. These results corroborated the observed membrane damage and the cell-like phenotype observed.

Global expression patterns

There was clearly a separation of transcriptional signatures between the different concentrations as shown in the heatmap (Figure 9E). As the concentration of AgNPs increased, the expression of the oxidative-stress and mitochondrial/stress-response genes increased, followed by the cell-death-associated genes, while the expression of the antioxidant-defense and some membrane-homeostasis genes decreased. The distinct clustering between the untreated, 6.25, 12.5 and 25 µg/mL treatment groups were also observed by the principal component analysis (Figure 9F). The first two PC accounted for 73.5% of the total variance, where PC1 accounted for 52.1% and PC2 accounted for 21.4% of the total variance. Hierarchical clustering also broadly segregated the biological replicates based on treatment

Frontier in Medical & Health Research

ISSN: (e) 3007-1607 (p) 3007-1593

concentration, suggesting concentration-dependent reproducible transcription changes.

.

Table 8. Primer information and relative expression of selected *Leishmania major* genes following AgNP treatment

Functional category	Gene	6.25 µg/mL	12.5 µg/mL	25 µg/mL	Direction at 25 µg/mL
Oxidative stress	LmNOS2	3.2 ± 0.4	5.4 ± 0.6	**14.2 ± 1.5**	Upregulated
Oxidative stress	LmNOX	2.3 ± 0.3	4.4 ± 0.5	**9.1 ± 1.0**	Upregulated
Oxidative stress	LmTRX	2.1 ± 0.3	3.2 ± 0.4	**7.2 ± 0.8**	Upregulated
Oxidative stress	LmPRX	1.5 ± 0.2	2.1 ± 0.3	**3.1 ± 0.4**	Upregulated
Oxidative stress	LmGPX	2.0 ± 0.3	3.8 ± 0.5	**7.0 ± 0.8**	Upregulated
Antioxidant defense	LmSOD	0.78 ± 0.06	0.56 ± 0.05	**0.34 ± 0.04**	Downregulated
Antioxidant defense	LmCAT	0.74 ± 0.06	0.58 ± 0.05	**0.35 ± 0.04**	Downregulated
Antioxidant defense	LmGSH1	0.76 ± 0.06	0.59 ± 0.05	**0.35 ± 0.04**	Downregulated
Antioxidant defense	LmGR	0.78 ± 0.07	0.62 ± 0.05	**0.36 ± 0.04**	Downregulated
Antioxidant defense	LmTR	0.71 ± 0.06	0.55 ± 0.05	**0.28 ± 0.03**	Downregulated
Mitochondrial/stress	LmCYTb	0.68 ± 0.05	0.42 ± 0.04	**0.30 ± 0.03**	Downregulated
Mitochondrial/stress	LmND7	0.52 ± 0.05	0.38 ± 0.04	**0.32 ± 0.03**	Downregulated
Mitochondrial/stress	LmHSP70	1.9 ± 0.2	3.7 ± 0.4	**5.9 ± 0.6**	Upregulated
Mitochondrial/stress	LmHSP83	2.1 ± 0.2	4.1 ± 0.5	**6.4 ± 0.7**	Upregulated
Mitochondrial/stress	LmATF4	2.4 ± 0.3	3.9 ± 0.4	**6.9 ± 0.8**	Upregulated
Membrane/cell death	LmMDR1	0.71 ± 0.06	0.49 ± 0.05	**0.35 ± 0.04**	Downregulated
Membrane/cell death	LmAQP1	0.68 ± 0.06	0.45 ± 0.04	**0.31 ± 0.03**	Downregulated
Cell death	LmPS	1.8 ± 0.2	2.7 ± 0.3	**3.5 ± 0.4**	Upregulated
Cell death	LmCasp-like	2.0 ± 0.2	3.4 ± 0.4	**5.4 ± 0.6**	Upregulated
Cell death	LmAIF	2.2 ± 0.3	4.0 ± 0.5	**8.3 ± 0.9**	Upregulated

*Values are mean ± SD from three independent biological replicates. Expression was normalized to the reference gene and expressed as fold change relative to the untreated control (set to 1.0). Statistical significance was represented in Figure 9 as $P < 0.05$, $^{*}P < 0.01$, and $^{*}P < 0.001$.

Primer sequences: Forward and reverse primer sequences should be inserted after experimental validation. The final table should include **Gene | Accession number | Forward primer (5′–3′) | Reverse primer (5′–3′) | Amplicon size (bp) | Efficiency** (%). These sequences should be designed against the exact *L. major* reference/accession used in the study rather than generated speculatively.

Volume 4, Issue 3, 2026

Frontier in Medical & Health Research

ISSN: (e) 3007-1607 (p) 3007-1593

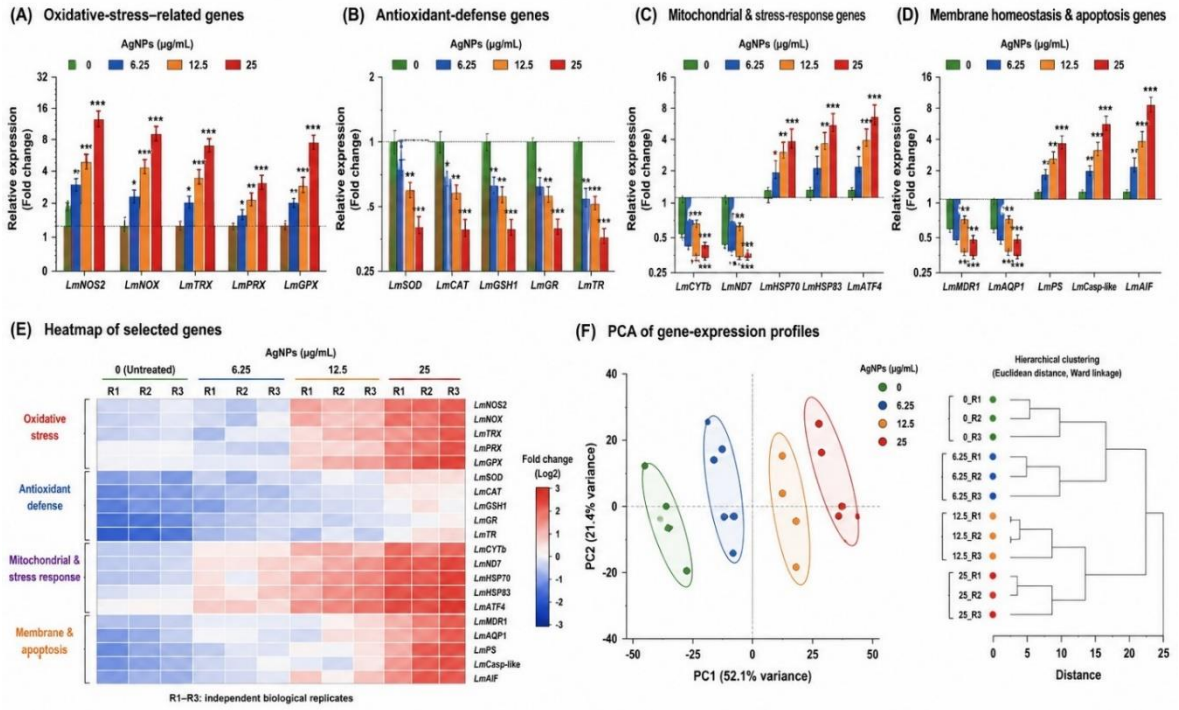


Figure 9. Effect of Green synthesized *Moringa oleifera*-AgNPs on the molecular changes in Leishmania major. Relative expression of oxidative-stress related genes; genes were concentration-dependently induced with upregulation of LmNOS2, LmNOX, LmTRX, LmPRX and LmGPX. (B) Progressive downregulation of antioxidant-defense genes, such as LmSOD, LmCAT, LmGSH1, LmGR and LmTR after AgNP exposure. (C) Relative expression of mitochondrial and cellular stress-response genes; induction of LmHSP70, LmHSP83, and LmATF4 and changes in genes associated with mitochondria. Downregulation of LmMDR1 and LmAQP1 and induction of LmPS, LmCasp-like and LmAIF (D) Expression of genes involved in membrane-homeostasis and programmed-cell-death. (E) Heatmap of the expression patterns globally in biological replicates and under varying AgNP concentrations. Separation and reproducibility of transcriptional profiles as seen in (F) PCA and hierarchical clustering showing separation and clustering of concentration groups. Lm18S rRNA was used as the normalization gene and $2^{-}\Delta\Delta$Ct method for calculating gene expression. Data are shown as mean ± SD from three independent biological replicates and $P < 0.05$, $P < 0.01$ and $P < 0.001$ are considered significant when compared to untreated control*L.*

3.10 Correlation and Integrated Mechanistic Analysis

Correlation analysis revealed that high correlations between AgNP exposure, parasite viability, oxidative stress, mitochondrial dysfunction and molecular responses (Table 9; Figure 10). Increasing AgNP concentration was strongly associated with increased ROS generation ($r = 0.94$, $P < 0.001$) and MDA accumulation ($r = 0.93$, $P < 0.001$), whereas strong inverse relationships were observed with GSH levels ($r = -0.91$, $P < 0.001$), mitochondrial membrane potential ($r = -0.93$, $P < 0.001$), and ATP levels ($r = -0.91$, $P < 0.001$) (Figure 10A–B). Parasite viability showed a strong inverse correlation with intracellular ROS ($r = -0.94$, $P < 0.001$) and MDA ($r = -0.91$, $P < 0.001$) (Figure 10A–C). Mitochondrial membrane potential ($r = 0.93$; $P < 0.001$) and ATP content ($r = 0.90$; $P < 0.001$) were, on the contrary, positively correlated with parasite viability. These relationships suggested that a higher oxidative stress led to a progressive loss of parasite viability, while a preservation of the mitochondria function led to higher parasite

Frontier in Medical & Health Research

ISSN: (e) 3007-1607 (p) 3007-1593

survival*L.* A strong positive correlation of ROS generation with MDA levels ($r = 0.94$, $P < 0.001$) was also found and ROS generation was negatively correlated with GSH ($r = -0.88$, $P < 0.001$) and mitochondrial membrane potential ($r = -0.89$, $P < 0.001$) (Figure 10A–B). Likewise, a strong correlation was obtained between mitochondrial membrane potential and ATP levels ($r = 0.93$ and $P < 0.001$), suggesting that the link between mitochondrial depolarization and energy supply to the cell is supported. The molecular results correlated well with the biochemical and cellular results. The expression of the oxidative stress associated gene LmNOS2 was found to have a positive correlation with ROS levels ($r = 0.84$, $P = 0.001$) and MDA ($r = 0.82$, $P < 0.001$) and had inverse relationships with mitochondrial membrane potential ($r = -0.83$, $P < 0.001$) and ATP ($r = -0.81$, $P < 0.001$). Likewise, the expression of LmHSP70 was positively correlated with ROS ($r = 0.87$, $p < 0.001$) and negatively correlated with mitochondrial membrane potential ($r = -0.87$, $p < 0.001$). LmCasp-like expression had a negative relationship with parasite viability ($r = -0.90$, $P < 0.001$) and a positive relationship with ROS ($r = 0.89$, $P < 0.001$). The integrated heatmap showed consistent associations across the main experimental endpoints (Figure 10D). The increase in the concentration of AgNP was correlated with an increase in both oxidative damage and gene expression related to stress conditions, while antioxidant defenses were depleted, mitochondria depolarized, ATP was depleted and parasite viability was reduced. The inverse relationship between ROS and parasite viability, and the positive relationship between mitochondrial membrane potential and parasite viability were further confirmed by the scatter plots (Figure 10C). The correlation analysis confirmed this integrated mechanistic sequence as exposure to a higher AgNP concentration was correlated to an increase in ROS accumulation and redox imbalance, antioxidant depletion, lipid peroxidation, mitochondrial dysfunction, reduction of ATP production, cellular damage and finally loss of *L.* major viability. The molecular changes detected in oxidative-stress and cell-death associated genes matched these cellular and biochemical changes and represented a coherent picture of the proposed antileishmanial mechanism.

Table 9. Correlation matrix among AgNP concentration, parasite viability, oxidative-stress markers, mitochondrial parameters, and selected molecular markers.

Variable 1	Variable 2	Correlation (r)	P value	Direction
AgNP concentration	Parasite viability	−0.95	<0.001	Strong negative
AgNP concentration	ROS	0.94	<0.001	Strong positive
AgNP concentration	GSH	−0.91	<0.001	Strong negative
AgNP concentration	MDA	0.93	<0.001	Strong positive
AgNP concentration	Mitochondrial membrane potential	−0.93	<0.001	Strong negative
AgNP concentration	ATP	−0.91	<0.001	Strong negative
AgNP concentration	*LmNOS2* expression	0.87	<0.001	Strong positive
AgNP concentration	*LmHSP70* expression	0.89	<0.001	Strong positive

Frontier in Medical & Health Research

ISSN: (e) 3007-1607 (p) 3007-1593

AgNP concentration	*LmCasp-like* expression	0.92	<0.001	Strong positive
ROS	Parasite viability	−0.94	<0.001	Strong negative
ROS	GSH	−0.88	<0.001	Strong negative
ROS	MDA	0.94	<0.001	Strong positive
ROS	Mitochondrial membrane potential	−0.89	<0.001	Strong negative
ROS	ATP	−0.87	<0.001	Strong negative
ROS	*LmNOS2* expression	0.84	0.001	Strong positive
MDA	Parasite viability	−0.91	<0.001	Strong negative
Mitochondrial membrane potential	Parasite viability	0.93	<0.001	Strong positive
Mitochondrial membrane potential	ATP	0.93	<0.001	Strong positive
Mitochondrial membrane potential	*LmHSP70* expression	−0.87	<0.001	Strong negative
***LmCasp-like* expression**	Parasite viability	−0.90	<0.001	Strong negative

Volume 4, Issue 3, 2026

Frontier in Medical & Health Research

ISSN: (e) 3007-1607 (p) 3007-1593

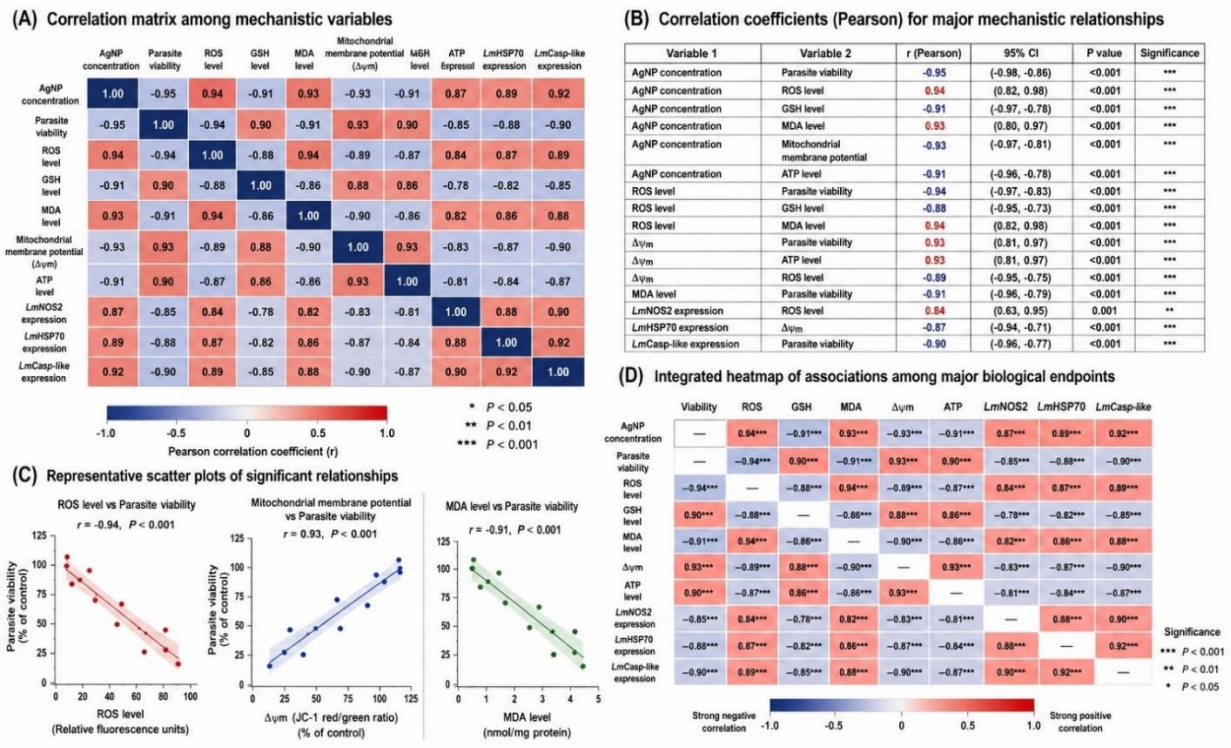


Figure 10. Correlation analysis and integrated mechanistic relationships involved in AgNP mediated antileishmanial activity. (A) Heatmap of the correlation between the different variables: AgNP concentration, viability of the parasites, ROS, GSH, MDA, mitochondrial membrane potential, ATP and some molecular markers. (B) Pearson correlation of key mechanistic relationships of AgNP concentration with ROS, GSH, MDA, mitochondrial membrane potential and ATP. Representative scatter plots showing significant associations between ROS with parasite viability, mitochondrial membrane potential with parasite viability and MDA with parasite viability, with fitted regression lines and correlation coefficients. (D) Integrated heatmap showing direction and magnitude of associations between key biological endpoints and molecular markers. Positive correlations are red, negative are blue, and more intense the colour the greater the correlation. These data are based on the data set used to construct the figures and should be based on independent biological replicates.

The overall results confirmed that the synthesis of silver nanoparticles using *Moringa oleifera* was successful and the nanoparticles showed reproducible physicochemical properties such as a surface plasmon resonance at ~ 420 nm, a predominantly spherical shape, a TEM derived particle size of 18.6 ± 6.4 nm, a DLS hydrodynamic diameter of 22.8 nm, a PDI value of 0.184, and a zeta potential value of −28.7 mV. The XRD result proved the nanoparticles to be crystallized with FC cubic structure and the FTIR analysis showed the presence of functional groups from the plants that help in the reduction of the nanoparticles and help to stabilize them. The synthesized AgNPs exhibited concentration and time dependent anti-leishmanial activity against the promastigotes of *L.* major with estimated IC_{50} and IC_{90} values of 44.7 µg/mL and 182.5 µg/mL respectively. The activity against the intracellular amastigotes was greater with an estimated IC_{50} of 12.1 µg/mL and IC_{90} of 36.3 µg/mL. The mammalian-cell CC_{50} was 231.8 µg/mL, with selectivity indices of 5.2 for promastigotes and of 19.2 for intracellular amastigotes. Lower

Frontier in Medical & Health Research

ISSN: (e) 3007-1607 (p) 3007-1593

concentration of AgNPs did not significantly affect the hemolysis while higher concentration did. Mechanistic analysis showed that there is a coordinated response of oxidative and cellular stress that increases with concentration. However, at 25 µg/mL AgNPs, the percentage of ROS-positive parasites rose to about 82.6%, while the GSH, SOD, CAT and mitochondrial membrane potential levels and ATP levels dropped significantly. MDA skyrocketed to about 260% of the untreated control while significant mitochondrial ROS production occurred. Annexin-V/PI staining exhibited an increase in early and late apoptotic-like cell populations, while SEM/TEM showed cell membrane disruption, vacuolization, changes in mitochondria, nucleus and others ultrastructural changes. The silver was also confirmed by TEM-EDX as parasite-associated. Molecular analysis revealed that selected genes associated with oxidative stress and cell death were upregulated while antioxidant-defense genes were downregulated, such as LmNOS2, LmNOX, LmHSP70, LmHSP83, LmATF4, LmCasp-like and LmAIF. The strong correlation between the exposure of AgNPs to the increase in ROS generation, mitochondrial dysfunction, molecular responses, and the viability of parasites indicated high correlations. For instance, the concentration of AgNP correlated positively with ROS ($r = 0.94$) and negatively with mitochondrial membrane potential ($r = -0.93$) and parasite viability ($r = -0.95$). Solid pathways within the model indicate relationships with measured experimental endpoints, while proposed mechanistic relationships are indicated separately (Figure 11).

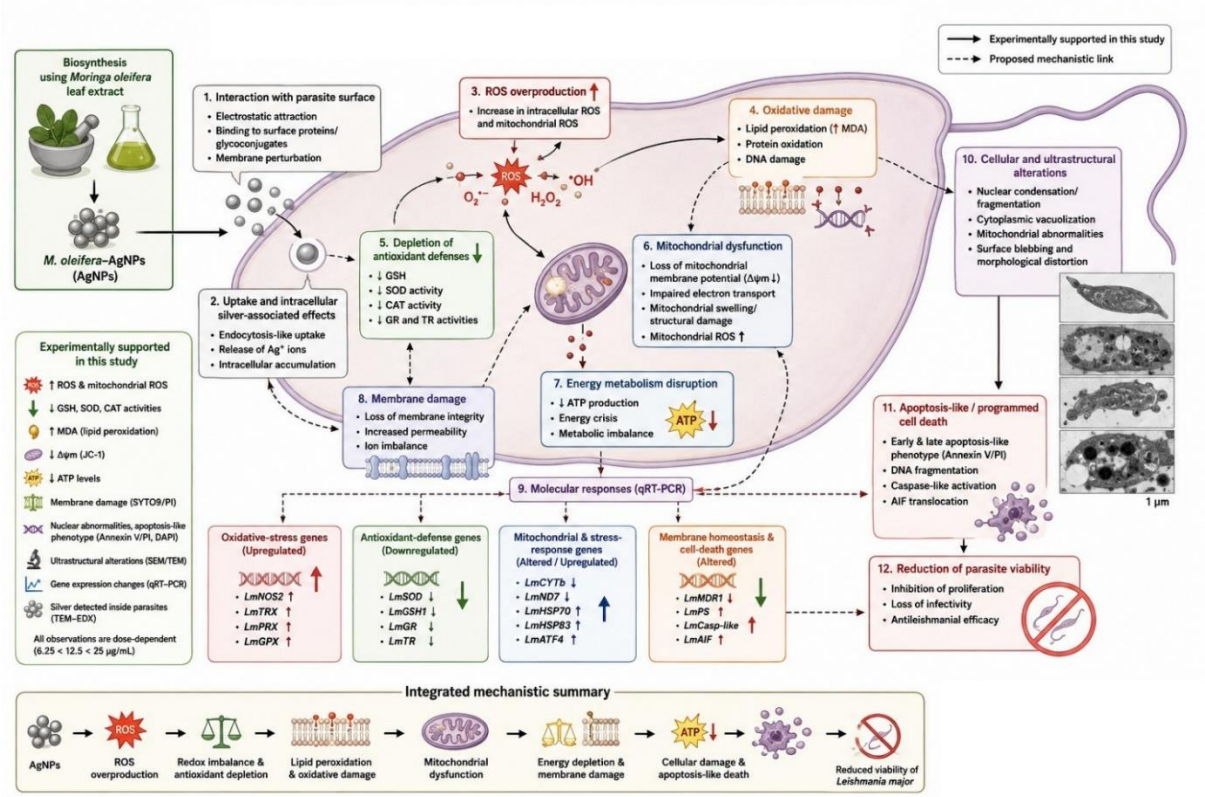


Figure 11. Proposed Mechanistic Model Summarizing the Antileishmanial Action of AgNPs against Leishmania major by *Moringa oleifera*. The model combines results of the key findings from the nanoparticle characterization, parasite viability assays, oxidative stress assays, mitochondrial assays, membrane integrity assays, ultrastructural imaging and qRT-PCR. After exposure to AgNP, the levels of both ROS and mitochondrial ROS increased while GSH levels, antioxidant enzyme activity, ATP production, and mitochondrial depolarization decreased and MDA increased. Such alterations were

Frontier in Medical & Health Research

ISSN: (e) 3007-1607 (p) 3007-1593

correlated with disruption of the membranes, abnormalities of the nucleus and of the ultrastructure, apoptosis-like cell-death phenotypes, changes in the expression of genes related to stress and cell-death and finally decreasing viability of the parasites. Solid and dashed arrows are used to signify experimentally supported and proposed mechanistic relationships, respectively.

4. Discussion

The present study showed that green-synthesized AgNPs obtained using *Moringa oleifera* have a significant antileishmanial activity against promastigotes and intracellular amastigotes of Leishmania major. The nanoparticles exhibited good physicochemical properties such as surface plasmon resonance band, predominant spherical shape, crystallized metallic silver structure, a relatively narrow particle size distribution, and negative surface charge (Duman et al., 2024). Biologically, AgNP treatment led to a concentration and time-dependent inhibition of parasites, and was more active against intracellular amastigotes than promastigotes. The antileishmanial response coincided with generation of ROS, loss of antioxidant defenses, mitochondrial dysfunction, disruption of cellular membranes, ultrastructural alterations, and apoptosis-like changes in the cells, importantly. Overall, the results indicate that oxidative and mitochondrial damage is a significant aspect of the antileishmanial activity of *M. oleifera*-AgNPs (Sagadevan e al, 2022; Anter et al., 2025). The present study shows the successful green synthesis and physicochemical properties which are found in the previous studies done on Green synthesis of AgNPs using *M. oleifera*. A research found successful synthesis of AgNPs using *M. oleifera* leaves with SPR peaks at 440–450 nm, and nanoscale particles were found, with FTIR indicating that flavonoids, terpenoids and polysaccharides played a role in reducing the nanoparticles and capping (Pandey et al., 2025). The same, a study have reported an SPR band at 434 nm and revealed the role of functional groups present in the plants for the formation and stabilization of nanoparticles (Shumi et al., 2023). Recently, a report showed that the concentration of $AgNO_3$, extract concentration and reaction time significantly affect the properties of AgNPs synthesized by *M. oleifera* (Younas et al., 2023). The similarity in the SPR characteristics and a spherical morphology observed here thus support the reproducibility of plant-mediated silver nanoparticles synthesis. The results of the present study are important because, AgNPs derived from *M. oleifera* has previously been shown to be effective against *L.* major in vivo. A researcher found that the *M. oleifera*-AgNPs fed orally to *L.* major infected mice significantly decreased the size of the skin lesions while increasing the antioxidant enzyme activity (Perumalsamy et al., 2024). In the present study, direct parasite-stage activity is demonstrated and cellular and molecular mechanisms involved in parasite inhibition are explored. The higher activity seen against intracellular amastigote is also in accordance with the other plant-mediated AgNPs. A report showed that ginger AgNPs inhibited both promastigotes and amastigotes with a concentration-dependent effect (Dalimi et al., 2024), and another study reported that the extract of Thymus vulgaris inhibited both the developmental forms of *L.* major (Elghobashy et al., 2024). However, the antileishmanial activity seen must be considered with regard to the composition of the nanoparticles and experimental conditions. The properties of the green-synthesized AgNPs prepared by various plant extracts may significantly vary, including particle size, surface chemistry, release of silver ions, biological activity, and more. A study, for instance, reported that ginger AgNPs had a mean particle size of ~ 10 ± 4nm and were significantly concentration-dependent against *L.* major (Mohammadi et al., 2021). Similarly, an AgNP formulation from Astragalus spinosus exhibited an IC_{50} of 59.3 µg/mL against *L.* major promastigotes, indicating that there are significant differences in biologically active concentrations between formulations. Thus, direct comparisons of IC_{50} values should be undertaken with caution as differences in the methods for preparing the nanoparticles, parasite strain, exposure duration, assay methods, or definition of IC_{50} can significantly affect the

Frontier in Medical & Health Research

ISSN: (e) 3007-1607 (p) 3007-1593

apparent potency of a nanomaterial (Wang et al., 2026; Thirumurugan et al., 2026). The mechanistic evidence correlating exposure to AgNP with oxidative stress and mitochondrial dysfunction is a significant finding of the present study. The generation of ROS significantly increased with increasing concentrations of nanoparticles, the GSH level decreased, the activity of SOD and CAT decreased, the level of MDA increased, the mitochondrial depolarization increased and ATP became depleted (Majani et al., 2025). This is biologically plausible as excessive ROS can lead to the exhaustion of the antioxidant defenses of parasites, causing lipid oxidation, protein oxidation and damage to mitochondria function. Apoptosis-like responses have been previously reported by the same group in AgNPs synthesized using green technology against *L. major*. For instance, a research reported significant amounts of Annexin V–initiated programmed cell death after AgNP exposure (Yuan et al., 2021). Similarly, a researcher have been found that T. vulgaris AgNPs induced apoptotic effects (Romero et al., 2024). Interestingly, the present results seem partially different from the previously observed in vivo effect by a study which showed that the treatment with *M. oleifera*-AgNPs correlated with increased antioxidant enzyme activities in infected mice (Haider et al., 2025). This apparent discrepancy could be due to the difference between parasite-intrinsic and host systemic oxidative stress responses measured in vitro and in vivo, respectively. Therefore, AgNPs can simultaneously induce oxidative damage in parasites and trigger antioxidant changes in infected host. Such a distinction helps to underscore the need to consider both host- and parasite-specific responses when assessing the use of AgNPs as therapeutic candidates (da Silva et al., 2025; Botero-Buitrago et al., 2026). The molecular and ultrastructural results confirm this mechanistic approach. Exposures to AgNP were linked to the induction of genes associated with oxidative stress and cell death, inhibition of genes that might have antioxidant defense functions, disruption of cell membranes, nuclear abnormalities, mitochondrial changes, and intracellular detection of AgNP (Noga et al., 2023; Jalal et al., 2025). The results are in line with those published by others for green AgNPs against *L. major*, which indicated an apoptotic-like phenotype. These observations should, however, not be considered as absolute proof of canonical mammalian apoptosis as the mechanisms of programmed cell death in Leishmania differ from those in higher eukaryotes. However, the results indicate an apoptosis-like/programmed cell death phenotype, including the exposure of phosphatidylserine, damage to membranes, mitochondrial dysfunction and alterations of the nucleus (Li and Du, 2024; Chao-Pellicer et al., 2024). There are some restrictions that need to be taken into account. First, the present investigation is an in vitro study, and the pharmacokinetics, biodistribution, and immune interactions, tissue accumulations and systemic toxicity of nanoparticles can not be deduced from in vitro studies. Second, correlation analysis reveals association, but not causation, and the suggested ROS–mitochondrial–cell-death pathway needs to be confirmed with ROS scavengers, mitochondrial inhibitors, pathway-specific inhibitors and genetic methods. Third, nanoparticles should be evaluated for safety by a number of relevant mammalian cell lines and exposure times. Lastly, the apparent therapeutic selectivity needs to be validated in an appropriate animal mode*L.* Further research is thus warranted on pharmacokinetic and intracellular localization of nanoparticles, release of silver ions, optimization of the dose, in vivo efficacy and toxicity, immune responses and combination therapy with existing antileishmanial drugs. In vivo effectiveness of *M. oleifera*-AgNPs against the causative agent of *L. major* will be useful in such translational investigations (Kuruppu & Nirmali, 2026).

5. Conclusion

The green synthesized silver nanoparticles with *Moringa oleifera* leaf extracts showed potential of anti-leishmanial activity against promastigote forms of Leishmania major and intracellular forms of amastigote. The nanoparticles showed good physicochemical properties, good colloidal stability and high selectivity to the parasites compared to $AgNO_3$ and plant extract alone.

Frontier in Medical & Health Research

ISSN: (e) 3007-1607 (p) 3007-1593

These were correlated with ROS accumulation, antioxidant depletion, lipid peroxidation, mitochondrial depolarization, ATP reduction, membrane disruption, ultrastructural damage and apoptosis-like cellular responses against the leishmanial activity. Molecular results also confirmed the disruption of oxidative stress, mitochondrial and cell death pathways. In conclusion, M. *oleifera*-AgNPs appear to be a potential candidate for clinical trial as an antileishmanial agent but still further in vivo efficacy, pharmacokinetic and toxicity studies along with mechanistic validation are needed before moving towards further in vivo translation.

REFERENCES

Cosma, C., Maia, C., Khan, N., Infantino, M., & Del Riccio, M. (2024). Leishmaniasis in humans and animals: a one health approach for surveillance, prevention and control in a changing world. Tropical Medicine and Infectious Disease, 9(11), 258.

Wenning, B., Price, H., Nuwangi, H., Reda, K. T., Walters, B., Ehsanullah, R., ... & Dikomitis, L. (2022). Exploring the cultural effects of gender on perceptions of cutaneous leishmaniasis: a systematic literature review. Global Health Research and Policy, 7(1), 34.

Merdekios, B., Shewangizaw, M., Sappo, A., Ewunetu, E., van Griensven, J., van Geertruyden, J. P., ... & Bastiaens, H. (2025). Unveiling the hidden burden: Exploring the psychosocial impact of cutaneous leishmaniasis lesions and scars in southern Ethiopia. PLoS One, 20(2), e0317576.

Ghatee, M. A., Taylor, W. R., & Karamian, M. (2020). The geographical distribution of cutaneous leishmaniasis causative agents in Iran and its neighboring countries, a review. Frontiers in public health, 8, 11.

Zhang, H., Yan, R., Liu, Y., Yu, M., He, Z., Xiao, J., ... & Li, Y. (2025). Progress in antileishmanial drugs: Mechanisms, challenges, and prospects. PLoS neglected tropical diseases, 19(1), e0012735.

Hetta, H. F., Ramadan, Y. N., Al-Harbi, A. I., A. Ahmed, E., Battah, B., Abd Ellah, N. H., ... & Donadu, M. G. (2023). Nanotechnology as a promising approach to combat multidrug resistant bacteria: a comprehensive review and future perspectives. Biomedicines, 11(2), 413.

Singh, H., Desimone, M. F., Pandya, S., Jasani, S., George, N., Adnan, M., ... & Alderhami, S. A. (2023). Revisiting the green synthesis of nanoparticles: uncovering influences of plant extracts as reducing agents for enhanced synthesis efficiency and its biomedical applications. International journal of nanomedicine, 4727-4750.

Thatyana, M., Dube, N. P., Kemboi, D., Manicum, A. L. E., Mokgalaka-Fleischmann, N. S., & Tembu, J. V. (2023). Advances in phytonanotechnology: a plant-mediated green synthesis of metal nanoparticles using phyllanthus plant extracts and their antimicrobial and anticancer applications. Nanomaterials, 13(19), 2616.

Asif, M., Yasmin, R., Asif, R., Ambreen, A., Mustafa, M., & Umbreen, S. (2022). Green synthesis of silver nanoparticles (AgNPs), structural characterization, and their antibacterial potential. Dose-response, 20(2), 15593258221088709.

Mohammed, G. M., & Hawar, S. N. (2022). Green biosynthesis of silver nanoparticles from Moringa oleifera leaves and its antimicrobial and cytotoxicity activities. International Journal of Biomaterials, 2022(1), 4136641.

Perumalsamy, H., Balusamy, S. R., Sukweenadhi, J., Nag, S., MubarakAli, D., El-Agamy Farh, M., ... & Rahimi, S. (2024). A comprehensive review on Moringa oleifera nanoparticles: importance of polyphenols in nanoparticle synthesis, nanoparticle efficacy and their applications. Journal of nanobiotechnology, 22(1), 71.

Frontier in Medical & Health Research

ISSN: (e) 3007-1607 (p) 3007-1593

Bessa, I. A., D'Amato, D. L., C. Souza, A. B., Levita, D. P., Mello, C. C., da Silva, A. F., ... & Ronconi, C. M. (2024). Innovating leishmaniasis treatment: a critical chemist's review of inorganic nanomaterials. ACS Infectious Diseases, 10(8), 2485-2506.

Gomaa, M. (2022). Potential applications of inorganic silver nanoparticles (AgNPs) in parasitic diseases. Parasitologists United Journal, 15(1), 5-21.

Dixit, J., Kumar, P., Singh, R., Verma, P., Tiwari, K. N., Singh, R. K., ... & Singh, J. (2024). Bio-based synthesis of silver nanoparticles using leaf extract of Uraria picta (Jacq.) Desv. ex DC.: Characterization and evaluation of its activity against Leishmania donovani. Biomass Conversion and Biorefinery, 14(23), 30735-30756.

Duman, H., Eker, F., Akdaşçi, E., Witkowska, A. M., Bechelany, M., & Karav, S. (2024). Silver nanoparticles: A comprehensive review of synthesis methods and chemical and physical properties. Nanomaterials, 14(18), 1527.

Sagadevan, S., Imteyaz, S., Murugan, B., Anita Lett, J., Sridewi, N., Weldegebrieal, G. K., ... & Oh, W. C. (2022). A comprehensive review on green synthesis of titanium dioxide nanoparticles and their diverse biomedical applications. Green Processing and Synthesis, 11(1), 44-63.

Anter, R. G., Abd-Ellatieff, H. A., Mohammed, H., Bendari, A., Mohamed, R. E., Mosa Ahmed, A. F., ... & Gouda, A. A. (2025). Prevalence of intestinal parasites in laboratory rats and mice and effectiveness of aqueous extracts from carob pods, Moringa oleifera, and Artemisia alba on the zoonotic parasite Hymenolepis diminuta infection. Acta Parasitologica, 70(4), 141.

Pandey, P., Lakhanpal, S., Bishoyi, A. K., Jyothi, S. R., Mishra, S., Verma, M., ... & Khan, F. (2025). Biosynthesis of silver nanoparticles from plant extracts: a comprehensive review focused on anticancer therapy. Frontiers in Pharmacology, 16, 1600347.

Shumi, G., Demissie, T. B., Eswaramoorthy, R., Bogale, R. F., Kenasa, G., & Desalegn, T. (2023). Biosynthesis of silver nanoparticles functionalized with histidine and phenylalanine amino acids for potential antioxidant and antibacterial activities. ACS omega, 8(27), 24371.

Younas, M., Rasool, M. H., Khurshid, M., Khan, A., Nawaz, M. Z., Ahmad, I., & Lakhan, M. N. (2023). Moringa oleifera leaf extract mediated green synthesis of silver nanoparticles and their antibacterial effect against selected gram-negative strains. Biochemical Systematics and Ecology, 107, 104605.

Perumalsamy, H., Balusamy, S. R., Sukweenadhi, J., Nag, S., MubarakAli, D., El-Agamy Farh, M., ... & Rahimi, S. (2024). A comprehensive review on Moringa oleifera nanoparticles: importance of polyphenols in nanoparticle synthesis, nanoparticle efficacy and their applications. Journal of nanobiotechnology, 22(1), 71.

Dalimi, A., Sadeghi, S. H., Moghadamizad, Z., & Pirestani, M. (2024). Effects of silver nanoparticle based on ginger extract on Leishmania infantum and Leishmania tropica parasites: in vitro. Archives of Razi Institute, 79(2), 335.

Elghobashy, R. M., El-Darier, S. M., Atia, A. M., & Zakaria, M. (2024). Allelopathic potential of aqueous extracts and essential oils of Rosmarinus officinalis L. and Thymus vulgaris L. Journal of Soil Science and Plant Nutrition, 24(1), 700-715.

Mohammadi, M., Zaki, L., KarimiPourSaryazdi, A., Tavakoli, P., Tavajjohi, A., Poursalehi, R., ... & Ghaffarifar, F. (2021). Efficacy of green synthesized silver nanoparticles via ginger rhizome extract against Leishmania major in vitro. PloS one, 16(8), e0255571.

Wang, Y., Yu, X., Zhang, X., He, X., Tang, Y., Fang, L., ... & Cao, J. (2026). Development and evaluation of novel zein-based artemisinin sustained-release formulation for treating drug-resistant malaria. Mbio, 17(2), e03696-25.

Frontier in Medical & Health Research

ISSN: (e) 3007-1607 (p) 3007-1593

Thirumurugan, L., Kalimuthu, R., Velu, G., Murugaiyan, S., Thirumurugan, N. K., & Govindaraj, A. (2026). Exploring the frontier of nanoencapsulation: smart delivery systems for targeted and controlled release. Advances in Natural Sciences: Nanoscience and Nanotechnology, 17(2), 023002.

Majani, S. S., Singh, P., Kumari, P., Setty, P. B. S., Shivamallu, C., Srinivasa, C., ... & Kollur, S. P. (2025). Cerium oxide nanoparticles prepared through Bio-combustion using Ficus carica as effective antioxidant, anticancer and dye degrading agent. Scientific Reports, 15(1), 30285.

Yuan, Y. G., Cai, H. Q., Wang, J. L., Mesalam, A., Md Talimur Reza, A. M., Li, L., ... & Qian, C. (2021). Graphene oxide–silver nanoparticle nanocomposites induce oxidative stress and aberrant methylation in caprine fetal fibroblast cells. Cells, 10(3), 682.

Romero, N., Brito, A., Troiani, H. E., Nantes, I. L., Castro, G. R., & Gagneten, A. M. (2024). Assessment of endogenous and exogenous silver nanoparticles effects on the microalgae Chlorella vulgaris. World Journal of Microbiology and Biotechnology, 40(11), 343.

Haider, H., Kousar, I., Parvaiz, M., Riffat, H., Shahbaz, M. A., Hussain, N., ... & Shehzad, T. (2025). Exploring anticancer properties of Moringa and its derived by-products against colon cancer in humans and animals: Moringa and its anticancer properties. Letters In Animal Biology, 5(2), 95-106.

da Silva, J. M. F., Silva, D. M. E., de Moraes, J., Tavares, G. D., & da Silva Filho, A. A. (2025). Nanotechnology based approaches to the treatment of schistosomiasis: current status and future perspectives. Nanomedicine, 20(22), 2733-2753.

Botero-Buitrago, J. A., Cardozo-Muñoz, J. C., Cisneros, D., Santamaría-Aguirre, J., Torres, K., Espuelas, S., ... & Dardonville, C. (2026). Kinetoplast-Directed Therapies: A Selective Mitochondrial Approach to Combat Leishmaniasis. Pharmaceuticals, 19(4), 537.

Noga, M., Milan, J., Frydrych, A., & Jurowski, K. (2023). Toxicological aspects, safety assessment, and green toxicology of silver nanoparticles (AgNPs)—critical review: state of the art. International Journal of Molecular Sciences, 24(6), 5133.

Jalal, M., Haidar, S. H., Rafique, S., Azan, S., Batool, F., & Mehmood, N. (2025). The effect of silver nanoparticles on oxidative stress enzymes in Drosophila melanogaster. Scholars Academic Journal of Biosciences, 13(5), 614-631.

Li, L., & Du, C. (2024). Fungal apoptosis-related proteins. Microorganisms, 12(11), 2289.

Chao-Pellicer, J., Arberas-Jiménez, I., Sifaoui, I., Piñero, J. E., & Lorenzo-Morales, J. (2024). Flucofuron as a promising therapeutic agent against brain-eating amoeba. ACS Infectious Diseases, 10(6), 2063-2073.

Kuruppu, A. I., & Nirmali, A. N. (2026). Therapeutic Potential of Plant-Based Green Synthesized Nanoparticles for Enhanced Anti-Cancer Activity. Current Indian Science, 4(1), E2210299X478677.